AMERICAN SOCIETY FOR MICROBIOLOGY | Molecular and Cellular Biology®

RESEARCH ARTICLE

Mnt Represses Epithelial Identity To Promote Epithelial-to-Mesenchymal Transition

Deborah P. Lavin,[a] Leila Abassi,[b] Mohammed Inayatullah,[a] Vijay K. Tiwari[a]

[a]Wellcome-Wolfson Institute for Experimental Medicine, School of Medicine, Dentistry & Biomedical Science, Queens University, Belfast, United Kingdom
[b]Department of Vaccinology and Applied Microbiology, Helmholtz Center for Infection Research, Braunschweig, Germany

ABSTRACT The multistep process of epithelial-to-mesenchymal transition (EMT), whereby static epithelial cells become migratory mesenchymal cells, plays a critical role during various developmental contexts, wound healing, and pathological conditions such as cancer metastasis. Despite the established function of basic helix-loop-helix (bHLH) transcription factors (TFs) in cell fate determination, only a few have been examined for their role in EMT. Here, using transcriptome analysis of distinct stages during stepwise progression of transforming growth factor beta (TGFβ)-induced EMT in mammary epithelial cells, we revealed distinct categories of bHLH TFs that show differential expression kinetics during EMT. Using a short interfering RNA-mediated functional screen for bHLH TFs during EMT, we found Max network transcription repressor (MNT) to be essential for EMT in mammary epithelial cells. We show that the depletion of MNT blocks TGFβ-induced morphological changes during EMT, and this is accompanied by derepression of a large number of epithelial genes. We show that MNT mediates the repression of epithelial identity genes during EMT by recruiting HDAC1 and mediating the loss of H3K27ac and chromatin accessibility. Lastly, we show that MNT is expressed at higher levels in EMT-High breast cancer cells and is required for their migration. Taken together, these findings establish MNT as a critical regulator of cell fate changes during mammary EMT.

IMPORTANCE The bHLH TF Mnt promotes epithelial to mesenchymal transition through epigenetic repression of the epithelial gene expression program.

KEYWORDS EMT, transcription factors, epigenetic mechanisms, gene regulation, breast cancers, cell biology, cell fate, epigenetics

Epithelial-to-mesenchymal transition (EMT) is a multistep process whereby polarized epithelial cells cease to maintain cell-to-cell contacts, lose characteristic epithelial cell markers, and acquire mesenchymal cell markers and properties such as motility, contractile ability, and invasiveness (1, 2). EMT is a dynamic reversible process involving a plethora of signaling pathways and transcription factors (TFs) (1). Epithelial cells undergoing EMT exhibit epithelial-mesenchymal plasticity, resulting in a spectrum of intermediate states expressing various levels of both epithelial and mesenchymal markers (2). EMT is employed in various contexts, including embryogenesis, organ development, and wound healing (1, 2). Furthermore, in addition to enabling tumor metastasis, EMT confers stemness, helps tumors evade immune destruction, and contributes to chemoresistance; therefore, EMT is of great therapeutic interest in cancer biology (3). The reverse process, MET (mesenchymal-to-epithelial transition), also occurs during embryogenesis and is required for secondary tumor formation (1, 4). Breast cancer is the most frequent cancer in women and is classified into four molecular subtypes that include luminal (A or B), human epidermal growth factor receptor 2 positive (HER2$^+$), and triple-negative breast cancer (TNBC) based on expression of the estrogen receptor (ER), progesterone receptor (PR), and HER2 protein abundance (5). Traditionally, TNBC, which presents with highly metastatic tumors and poor prognosis/treatment response (6, 7), is the molecular subtype of breast cancer that is associated with EMT,

Citation Lavin DP, Abassi L, Inayatullah M, Tiwari VK. 2021. Mnt represses epithelial identity to promote epithelial-to-mesenchymal transition. Mol Cell Biol 41:e00183-21. https://doi.org/10.1128/MCB.00183-21.

Address correspondence to Vijay K. Tiwari, v.tiwari@qub.ac.uk.

Received 23 April 2021
Returned for modification 18 May 2021
Accepted 20 August 2021
Accepted manuscript posted online 30 August 2021
Published 26 October 2021

with EMT marker expression significantly higher in particular subgroups of TNBC (8). A universal EMT scoring system for multiple cancers, including breast, ovarian, and gastric, has previously been established and suggests that each cancer has its inherent spectrum of EMT (9).

Transforming growth factor beta (TGFβ) is the canonical EMT inducer, and several studies, including ours, have used TGFβ-induced EMT models to elucidate the roles of extracellular stimuli, intracellular signaling pathways, TFs, epigenetic modifications, and chromatin remodeling machinery in EMT (10–20). The established and most widely studied EMT-promoting TF families are Snail, Zeb, and Twist, which bind to regulatory elements in the genome and work in unison with epigenetic regulators (such as G9a and LSD1) and chromatin remodeling machinery to drive transcription of promesenchymal genes and prevent epithelial gene transcription (21). Several studies (reviewed in reference 22), including previously published data from our lab, concluded that rewiring of the gene regulatory program is essential in driving distinct events during EMT (11, 13–15, 20).

The basic helix-loop-helix (bHLH) family of dimeric transcriptional regulators are established inducers of cell fate determination in a variety of contexts, including neurogenesis (NeuroD1 [20, 23] and Math-1), cardiogenesis (dHAND and eHAND), myogenesis (MyoD and MyF5) and hematopoiesis (SCL; stem cell leukemia) (24), as well as disease states such as cancer (DEC1 and DEC2 [25] and HEY1 [26]). Among bHLH TFs, Twist1 and Twist2, Tcf3 (also known as E12 and E47), Tcf4, and Tcf12 are known to regulate EMT (27). bHLH TFs can act as transcriptional activators or repressors by recruiting histone acetyltransferases (HAT) (p300 or SAGA complex) or corepressors such as Groucho or SIN3A, respectively (27, 28). Working together with epigenetic mediators and chromatin remodeling machinery, they drive/repress transcription of their target genes (21, 29, 30). For example, TWIST1 represses *CDH1* expression by recruiting MBD1 (methyl-CpG-binding domain protein 1) or PRC1 subunits (Bmi1) (21). Despite the diverse roles of bHLH TFs in cell cycle regulation, differentiation, development, and tumorigenesis, no studies thus far have specifically focused on investigating the dynamics of bHLH TF expression during EMT to identify further EMT-relevant bHLH TFs. In this study, we found that Max network transcription repressor (MNT; also known as ROX, MAD6, or MXD6), a member of the Mad family within the bHLH TF family (31), is critical for EMT in mammary epithelial cells. MNT is widely induced during EMT, and its depletion during this process prevented the repression of many epithelial genes. This was accompanied by severe inhibition of hallmark EMT morphological changes. Mechanistically, MNT promotes EMT through HDAC1-mediated epigenetic remodeling and repression of epithelial identity-related genes during EMT. Lastly, MNT and its target genes are highly expressed in EMT-High breast cancers and MNT is required for breast cancer cell migration. These observations establish MNT as a novel essential regulator of EMT in mammary epithelial cells.

RESULTS

Analysis of expression kinetics of bHLH TFs during mammary EMT identifies MNT as a critical regulator of this process. To analyze the expression kinetics of bHLH TFs during EMT in mammary epithelial cells, our workflow (Fig. 1a) included transcriptome analysis of data derived from two well-established *in vitro* models, which use either normal murine mammary gland epithelial (NMuMG) cells or human mammary epithelial (HMLE) cells. NMuMG cells were treated with TGFβ for up to 10 days to recapitulate early (day 1), intermediate (EMP; day 4, day 7), and late (day 10) stages of EMT. For HMLE cells, two additional time points (day 15 and day 20) were included, as human epithelial cells require more time to accomplish EMT than murine epithelial cells. Using the transcriptome data derived from the indicated time points during mouse (15) and human (available as accession no. GSE99722) EMT, we investigated the kinetics of all known bHLH TFs (32). In the murine system, we observed three clusters of bHLH TF expression; a large number showed a decrease in expression during EMT (Fig. 1b, cluster 3), while others either increased as EMT progressed (Fig. 1b, cluster 1) or showed fluctuations in expression as cells became more mesenchymal in nature (Fig. 1b, cluster 2). Similar dynamics were observed in the human system, with many bHLH TFs decreasing as cells lost their epithelial properties (Fig. 1c, clusters 2 and 5), with other bHLH TFs showing variable (Fig. 1c, clusters 1, 3, and 4) or increasing expression as EMT

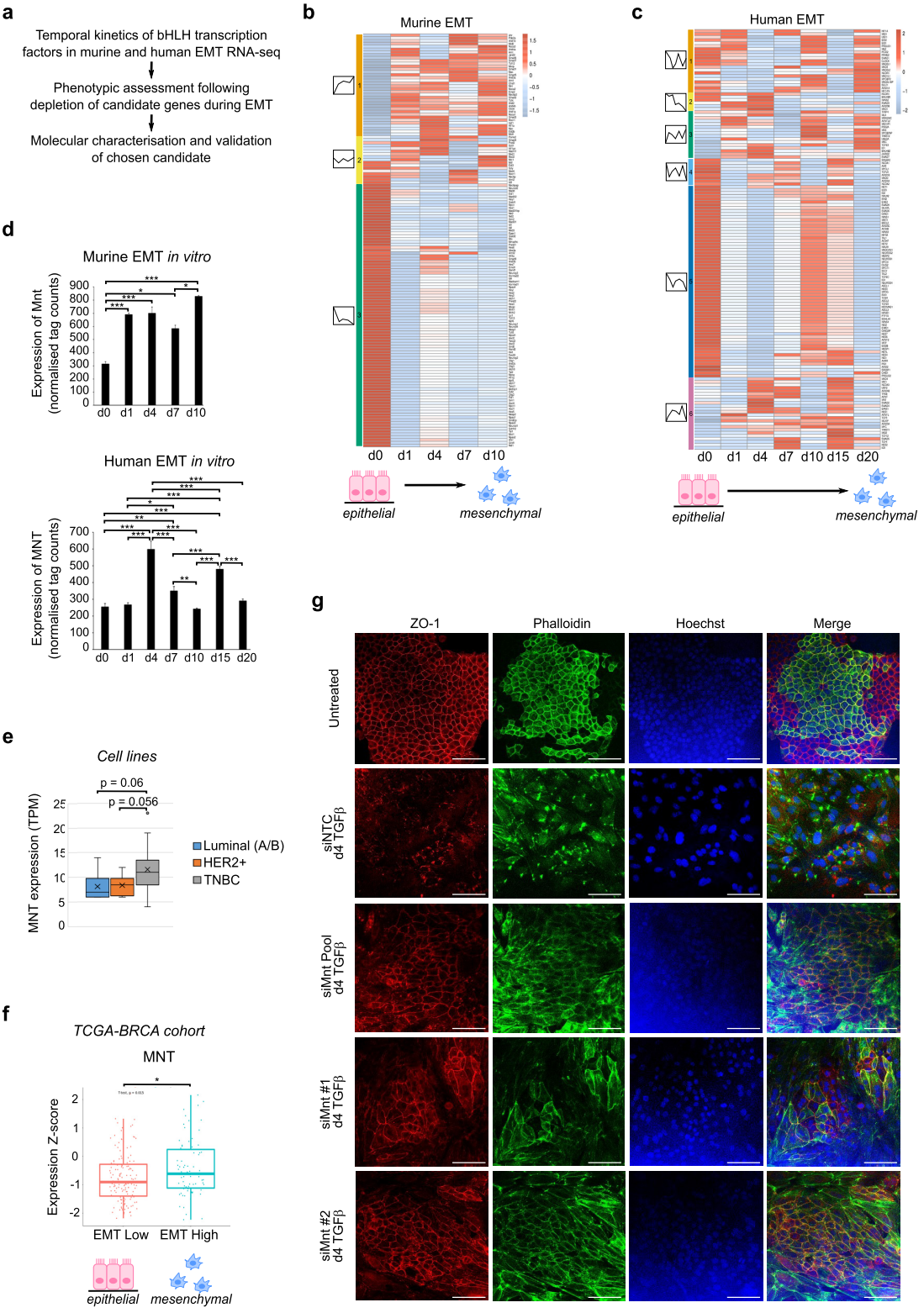

FIG 1 MNT is a novel essential regulator of cell fate changes during EMT. (a) Schematic representation of the workflow involved in the identification of bHLH TFs that are critical for EMT, using our *in vitro* EMT model systems. (b) Heatmap showing normalized tag counts (average from three replicates per time point) of all known bHLH TFs in murine NMuMG cells undergoing TGFβ-induced EMT *in vitro* for the indicated times. Schematic depictions of epithelial, transitionary (arrow), and mesenchymal cell states are indicated below the corresponding time points. Different colored boxes represent candidates in clusters 1 to 3, and line graphs depict cluster dynamics. (c) As for panel a, but in human HMLE cells with six clusters identified. (d) Murine Mnt (top) and human MNT (bottom) expression dynamics as normalized tag counts derived from RNA-seq data from TGFβ-induced EMT *in vitro*. (e) MNT

(Continued on next page)

progressed (Fig. 1c, cluster 6). In both model systems, the most dramatic change in temporal kinetics was observed from day 0 to day 1, potentially because epithelial cells massively reprogram their transcriptome in response to TGFβ and begin to acquire a mesenchymal identity. We were most interested in those bHLH TFs whose expression increased with TGFβ treatment, since these TFs may be involved in promoting mesenchymal gene expression and EMT-related phenotypic changes, whereas bHLH TFs that decreased during EMT likely have a role in epithelial cell maintenance.

We selected a preliminary list of 45 candidates (see Fig. S1a, left, in the supplemental material) for our initial screen. We chose candidates that showed comparable expression dynamics in murine and human EMT. Based on the published literature about these candidates and their expression patterns in these model systems, we subsequently shortlisted 19 bHLH TFs that were not previously studied in the context of EMT and either highly expressed or showed changes in transcriptional dynamics during EMT (Fig. S1a, right). Of these 19 candidate bHLH TFs, six showed decreased expression at each stage of TGFβ treatment compared to untreated epithelial cells (Fig. S1a, cluster 2, right), which suggests that these candidates are crucial to epithelial identity. We proceeded to perform short interfering RNA (siRNA)-mediated candidate knockdown during TGFβ-induced EMT and assessed the cellular phenotype after 4 days (Fig. S1b). Regarding candidates whose expression decreased during EMT, morphological examination revealed that individual depletion of bHLH TF Mlx or Srebf1 appeared to accelerate the acquisition of a mesenchymal phenotype, while knockdown of Mxd3, Srebf2, Tcfeb, or Tcfec appeared to enhance cell death (Fig. S1b). This suggests that Mlx and Srebf1 are key epithelial TFs. In terms of cellular morphology, depletion of most of the candidates had no significant effect; only knockdown of Mlxip or Mxi1 during EMT resulted in elongated cells, a classic characteristic acquired by cobblestone epithelial cells undergoing EMT (Fig. S1b, Table S1). Increased cellular proliferation was only observed following depletion of four candidates, Mlxip, Mnt, Mxi1, or Tcf3, where Tcf3 was included as a positive control to show immediate inhibition of EMT upon depletion of this known *CDH1* repressor and EMT inducer (27). Based on our available data, it is likely that the knockdown of Mxd4, Neurod6, or Usf1 caused increased apoptosis (Fig. S1b, Table S1), which agrees with previous findings on Neurod6. In the absence of Neurod6, Neurod6$^+$ neurons in the ventral tegmental area die from apoptosis at early postnatal stages (33), and Neurod6 prevents caspase-3 activation upon serum deprivation by triggering expression of antiapoptotic BclII members (34). Depletion of bHLHa15, Mnt, or Mxd1 during TGFβ-induced EMT inhibited EMT in NMuMG cells (Fig. S1b, Table S1). Among these three factors, we chose Mnt for subsequent experimental validation, as its knockdown, validated by Western blotting (Fig. S1c) and reverse transcription-quantitative PCR (RT-qPCR) (Fig. S1d), consistently gave the strongest reversal of the EMT phenotype. In addition, Mnt depletion in untreated epithelial cells increased E-cadherin protein expression (Fig. S1c), which suggested a role for MNT in epithelial gene regulation. Since EMT is also closely associated with resistance to proapoptotic stimuli, we also examined the effect of Mnt depletion on ionizing radiation (iR) sensitivity in NMuMG cells. Unstained NMuMG cells transfected with siNTC or siMnt were weakly positive for annexin V, as expected (Fig. S2a and b, respectively). We observed that Mnt depletion enhanced NMuMG sensitivity to iR, as shown by more annexin V (a marker of apoptotic cells)-positive cells in siMnt (Fig. S2e, f, g) versus the nontargeting control (siNTC) (Fig. S2b, c, g).

FIG 1 Legend (Continued)
expression (as transcripts per million) was plotted in cell lines that reflect molecular subtypes of breast cancer, luminal (blue bars, $n = 8$), HER2$^+$ (orange bars, $n = 8$), and TNBC (gray bars, $n = 21$). (f) Representative box plot showing normalized expression of MNT in selected TCGA-BRCA tumor samples categorized as EMT Low and EMT High based on a 12-EMT-gene signature. The *y* axis represents the normalized Z score. (g) Representative immunofluorescence images showing the localization and expression levels of EMT marker proteins after 4 days of siRNA-mediated depletion of Mnt (pool of four siRNAs or two individual siRNAs) compared to the nontargeting control (siNTC) in NMuMG cells. Immunofluorescent staining was performed with antibodies against the epithelial marker ZO-1 and phalloidin (to visualize the actin cytoskeleton). Images were acquired at 40×. Scale bars represent 100 μm. Error bars represent the means ± SEM from three independent biological replicates ($n = 3$). *, $P < 0.05$; **, $P < 0.01$; ***, $P < 0.001$; one-way ANOVA with Bonferroni multiple-comparison test (d and e) or unpaired two-tailed Student's *t* test (f), alpha = 0.05. See also Fig. S1, S3, and S4.

Human MNT and mouse Mnt exhibit 89% and 93% identity at mRNA and protein levels, respectively (NCBI BLAST) (Tables S2 and S3, respectively). MNT expression in our transcriptome data (15) derived from our respective human and murine *in vitro* EMT models showed comparable dynamics with increased MNT during EMT (Fig. 1d). To determine how Mnt upregulation correlated with the decrease and increase of epithelial (Cdh1 and Tjp1) and mesenchymal (Fn1, Vim) genes, respectively, we examined these genes in the same murine and human transcriptome data (Fig. S3a and d, respectively) and observed similar dynamics between Mnt and Fn1 in both systems. We also performed Western blot analysis of fibronectin, E-cadherin, and Mnt during TGFβ-induced EMT in murine and human *in vitro* models (Fig. S3b and c and e and f). Despite the high similarity between human and murine Mnt at the protein level, we faced detection issues via Western blotting using four commercially available Mnt antibodies (detailed in Materials and Methods). However, we were able to detect Mnt in our EMT *in vitro* models, where we saw that Mnt expression mimicked the dynamics observed in transcriptome sequencing (RNA-seq), with peak Mnt observed at day 4 in murine (Fig. S3b and c) and day 10 in human (Fig. S3e and f) epithelial cells undergoing EMT. Given these preliminary data and our hypothesis that MNT is a pro-EMT TF, we assessed its expression in cell lines that reflect the different molecular subtypes of breast cancer (Table S4). We observed a trend toward higher expression in TNBC ($n = 21$ cell lines) versus both HER2$^+$ ($n = 8$) and luminal A/B ($n = 8$) subtypes (Fig. 1e), which suggests that MNT is highly expressed in aggressive molecular subtypes of breast cancer, which are known for their invasiveness and metastatic ability. This agrees with our proposed pro-EMT role of MNT, as EMT is traditionally associated with the most aggressive molecular subtype, TNBC. For further validation, we examined MNT expression in an extensive breast cancer primary tumor cohort from The Cancer Genome Atlas (TCGA-BRCA) cohort containing 1,102 patients. First, we classified the TCGA-BRCA cohort into EMT Low (i.e., epithelial) or EMT High (i.e., mesenchymal) according to the EMT status using established EMT markers (epithelial, *ESRP1*, *ESRP2*, *OVOL1*, *OVOL2*, and *CLDN3*; mesenchymal, *ZEB1*, *ZEB2*, *SNAI2*, *TWIST2*, *RBFOX2*, and *FN1*) (Fig. S4a). Further analysis of MNT expression in these two groups revealed a significantly higher MNT expression in EMT High versus EMT Low (Fig. 1f).

Next, we aimed to further characterize aberrations in morphological features of EMT following siRNA-mediated depletion of Mnt during EMT using immunofluorescence (IF) assays for established markers. In control siRNA-treated cells undergoing EMT (siNTC), we observed the expected reduced ZO-1 staining, actin filament reorganization, and cytoskeletal remodeling, as evidenced by phalloidin staining (Fig. 1g, second column). Depletion of Mnt (siMnt; pool of four siRNAs or individual siRNAs) during EMT blocked this process, with immunofluorescence staining of these cells comparable to that of untreated epithelial cells. For example, cells lacking Mnt during EMT retained their epithelial cell tight junctions (ZO-1) (Fig. 1g, third, fourth, and fifth columns), confirming that Mnt is a critical regulator of EMT. Cytoskeletal remodeling was also reduced, as shown by comparable phalloidin staining in untreated (Fig. 1g, first column) and siMnt during EMT, indicating retention in the epithelial state. In terms of cell size and morphology, we also measured individual cell length and width (Fig. S4b, top and middle, respectively) and calculated the spindle index (SI) (Fig. S4b, bottom) as previously described (35–37). We observed a significant increase in cell length, cell width, and subsequent SI in siNTC during EMT versus untreated cells, which is consistent with the acquisition of a mesenchymal phenotype. However, the depletion of Mnt during EMT inhibited such morphological changes, with cell length, cell width, and SI measurements comparable to those of the untreated epithelial cells. In agreement with our immunofluorescence data, we detected increased E-cadherin expression following depletion of Mnt during EMT (Fig. S4c).

Altogether, these comprehensive sets of data suggest that Mnt is critical for phenotypic and molecular changes underlying EMT in mammary epithelial cells.

MNT promotes EMT by repressing epithelial and promoting mesenchymal programs. We next attempted to characterize the global molecular program governed by Mnt to regulate EMT. Toward this, we proceeded to characterize genome-wide aberrations in the gene expression program using RNA-seq assay following depletion of Mnt during EMT (Fig. 2a). Analysis of these RNA-seq data revealed a large number of

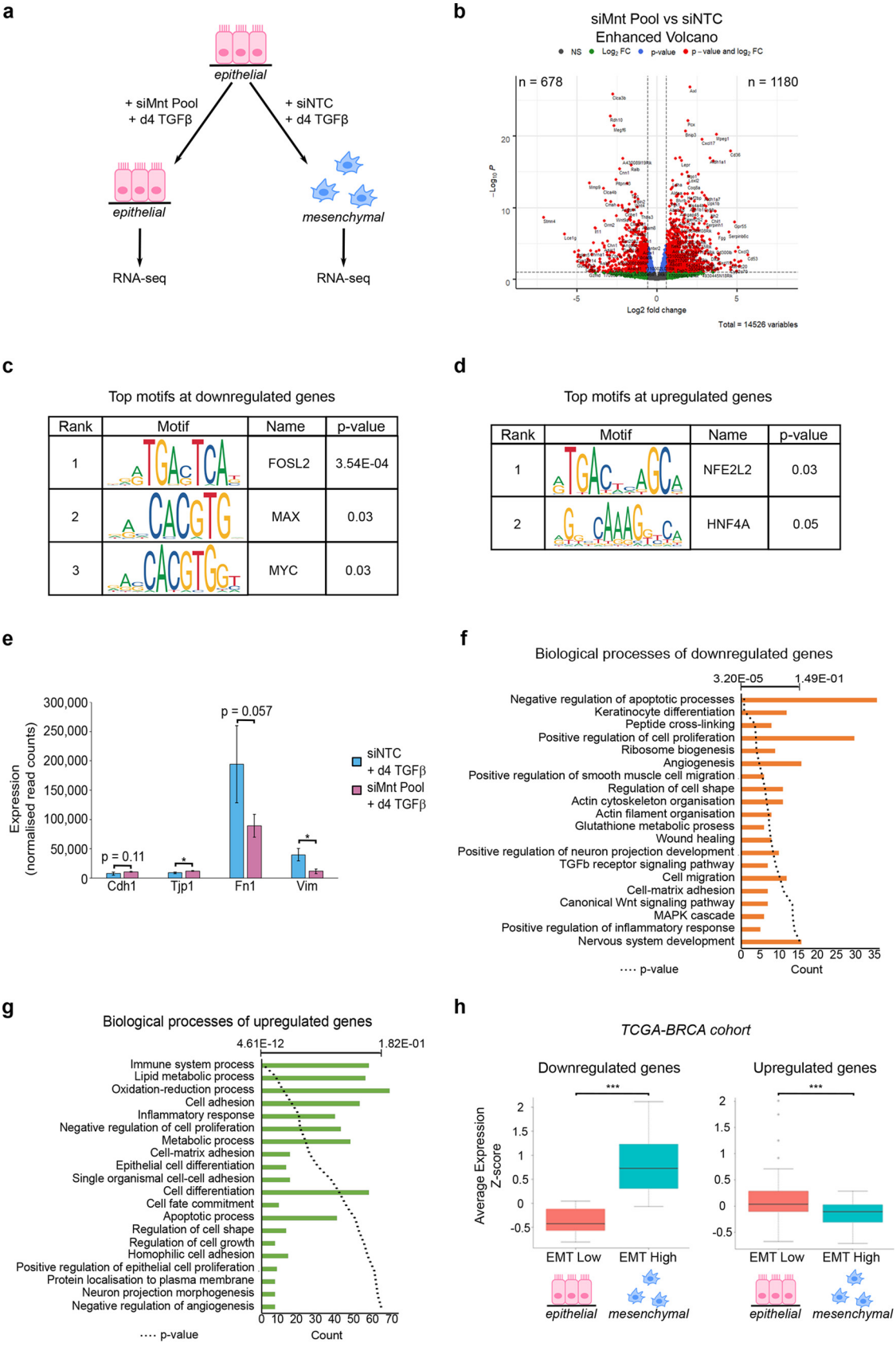

FIG 2 MNT represses epithelial cellular processes during EMT and increases promesenchymal gene expression. (a) Schematic representation of the experimental procedure. (b) Volcano plots showing significantly differentially expressed genes upon Mnt depletion in NMuMG cells undergoing EMT. (c and d) Tables depicting

(Continued on next page)

significantly differentially expressed genes (n = 678 downregulated, n = 1,180 upregulated) following the loss of Mnt during EMT (Fig. 2b). A higher number of upregulated genes suggested its potential repressive function during EMT, in line with previous reports (38–40). Interestingly, the downregulated genes were enriched for motifs of known EMT inducers, such as FOSL2, SMAD4, MYC, TCF3, and EGR1 (Fig. 2c and Table S6) (27, 41–44), while upregulated genes were enriched for motifs of NFE2L2 and HNF4A, which are known repressors of Snail-mediated pro-EMT transcription (Fig. 2d and Table S6), suggesting that the Mnt-governed gene regulatory program interacts with the core EMT program controlled by other key TFs. Examination of well-known EMT markers in the RNA-seq data revealed a significant increase in Tjp1 (ZO-1) and a significant decrease in vimentin upon Mnt depletion during EMT versus siNTC (Fig. 2e). Gene ontology (GO) analysis revealed that downregulated genes were enriched for pro-EMT and tumorigenic processes like angiogenesis, actin filament organization, cell migration, and negative regulation of apoptosis, among others (Fig. 2f), while upregulated genes showed enrichment for various metabolic processes, cell adhesion, epithelial cell differentiation, and regulation of cell growth, among other biological processes implicated in epithelial cell maintenance (Fig. 2g). KEGG pathways associated with upregulated and downregulated genes included cell adhesion molecules and focal adhesion, respectively (Fig. S5a and b).

To further shortlist potential critical Mnt target genes, we plotted the most significantly differentially expressed genes following siMnt in our EMT time courses, only keeping the downregulated genes that increased during EMT and upregulated genes that decreased during EMT (Fig. S5c and d). The downregulated genes contained well-known pro-EMT genes, such as *BMP1*, *FN1*, *MMP2*, *MMP9*, *SERPINE1*, and *ANGPTL2*, and one of the core EMT TFs, ZEB2, while the upregulated genes included the epithelial marker *MUC1*, the transmembrane protein gene *TMEM169*, and the TF *E2F2*, among many metabolic genes. Interestingly, Mnt also seems to repress several metabolic genes during EMT (Fig. S6a and b). Prompted by these observations, we next sought to determine whether such gene expression kinetics are relevant in cases of aberrant EMT. We subsequently plotted the shortlisted Mnt target genes in the TCGA-BRCA cohort reclassified according to EMT status. Genes that were downregulated upon Mnt knockdown (implicated in pro-EMT processes) showed increased expression in EMT-High versus EMT-Low breast cancer patients, while the genes upregulated upon Mnt knockdown (involved in cell adhesion, among other processes) were increased in EMT-Low versus EMT-High (Fig. 2h and Fig. S6c and d). These observations are in line with increased MNT expression in EMT-High primary breast tumors (Fig. 1f).

These observations clearly show that Mnt functions to repress the epithelial gene expression program and induce the mesenchymal transcriptional program to promote EMT.

MNT is essential for cellular migration, and single-nucleotide polymorphisms (SNPs) in its target genes are associated with EMT-related pathologies. We next tested whether MNT alone could enhance TGFβ-induced EMT by overexpressing green fluorescent protein (GFP)-MNT or empty vector (EV) control during EMT (Fig. 3a, left) and assessing the cellular phenotype. Here, GFP-MNT localized to the nucleus, whereas EV (which also contains GFP) showed cytoplasmic localization, further confirming Mnt as a nuclear protein (Fig. 3a, right). Interestingly, upon MNT overexpression, cells undergoing EMT became noticeably more elongated (Fig. 3b). To quantify this, we measured individual cell length and cell width and calculated the SI as explained earlier (Fig. 3c). Interestingly, while we observed comparable cellular dimensions between TGFβ and EV controls, we found a significant increase in SI upon MNT overexpression during EMT (Fig. 3c). This was further

FIG 2 Legend (Continued)
the most significantly enriched motifs at siMnt downregulated (c) and upregulated (d) genes determined using Enrichr. (e) Expression (as normalized read counts) of well-known EMT genes Cdh1, Tjp1, Fn1, and Vim in our RNA-seq data from siNTC or siMnt during TGFβ-induced EMT *in vitro*. (f and g) GO analysis of downregulated (f) and upregulated (g) genes upon Mnt knockdown in NMuMG cells that underwent EMT for 4 days. (h) Box plot depicting the average expression (Z scores) of MNT target genes in EMT-Low and EMT-High. *, $P < 0.05$; ***, $P < 0.001$; unpaired two-tailed Student's t test, alpha = 0.05. See also Fig. S5 and S6.

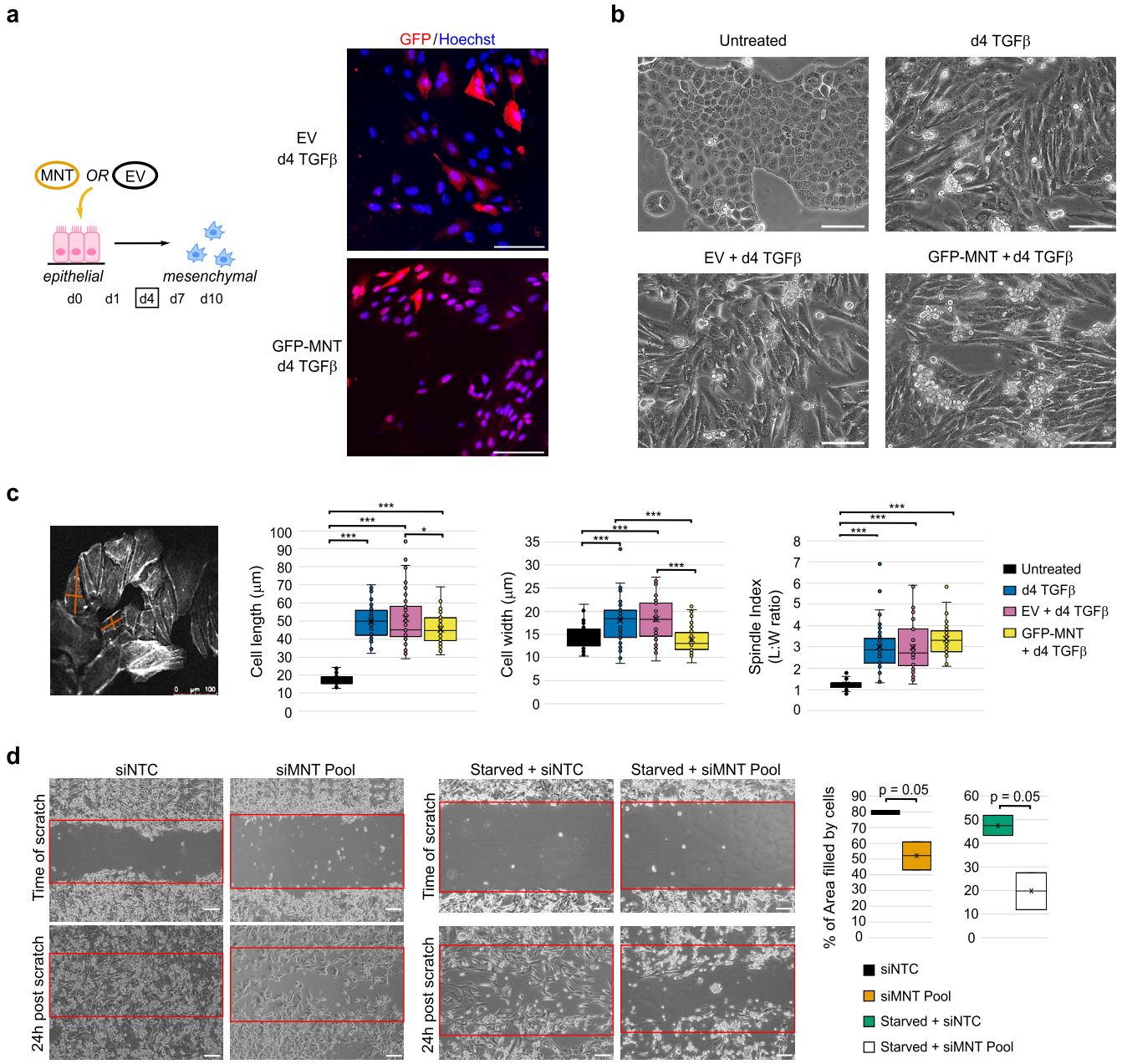

FIG 3 MNT is essential for cellular migration, and SNPs in its target genes associate with EMT-related pathologies. (a, left) Schematic representation of the experimental procedure. Representative immunofluorescence images (right) show the localization of empty vector control (EV, top) or GFP-tagged MNT (bottom) in NMuMG cells after 4 days of overexpression during EMT. Immunofluorescent staining was performed with antibodies against GFP and Hoechst. Transfection efficiency was measured by the presence of nuclear GFP. Images were acquired at 40×. (b) Representative bright-field images of untreated NMuMG cells and NMuMG cells subjected to 4 days of TGFβ or transfected with EV or GFP-MNT for 4 days during EMT, ×20 magnification. (c, first image) Example of how cell morphology/elongation quantification was performed using ImageJ. Box plots depict quantification of cell length (second) and cell width (third) as micrometers and the SI (fourth) for untreated (black), day 4 TGFβ treated (blue), EV plus day 4 TGFβ (pink), and GFP-MNT plus day 4 TGFβ (yellow). (d) Representative bright-field images of scratch wound assay in nonstarved (left) and starved (center) MDA-MB-231 cells treated for 4 days with siControl or siMNT. Images were taken at the time of scratch and 24 h after, ×10 magnification. After 24 h, the percentage of wound area occupied by cells was measured (right) for nonstarved siNTC (black), nonstarved siMNT (orange), starved siNTC (green), and starved siMNT (white) using the MRI wound healing tool in Image J. Scale bars represent 100 μm. *, $P < 0.05$; ***, $P < 0.001$; one-way ANOVA with Bonferroni multiple-comparison test (c and d), alpha = 0.05.

accompanied by a significant decrease in CDH1 expression (Fig. S6e). These observations imply that MNT can accelerate TGFβ-induced EMT.

To functionally validate MNT as a pro-EMT TF in TNBC, we depleted MNT in a TNBC breast cancer cell line, MDA-MB-231, and assessed cellular migration via wounding migration assays. In MDA-MB-231 cells lacking MNT, we observed a significant decrease in cells within the

TABLE 1 SNPs associated with genes upregulated upon siMnt (from Fig. 2) and implicated in EMT-related diseases

Gene	SNP	Consequence	EMT-related process
DIO1	rs2235544	Intron variant	Breast carcinoma
MUC1	rs753535070	Missense variant	Breast carcinoma
PPARG	rs1801282	Missense variant	Liver fibrosis
PPARG	rs1801282	Missense variant	Breast carcinoma
PPARG	rs1801282	Synonymous variant	Breast carcinoma
PPARG	rs3856806	Intron variant	Breast carcinoma
SCNN1A	rs5742912	Missense variant	Cystic fibrosis
SCNN1A	rs7973914	Intron variant	Breast carcinoma
SFTPD	rs721917	Missense variant	Cystic fibrosis
NQO1	rs1020475809	Synonymous variant	Breast carcinoma
NQO1	rs1258159645	Missense variant	Breast carcinoma
NQO1	rs1800566	Missense variant	Breast carcinoma

wound area versus control (Fig. 3d). In other words, depletion of MNT in MDA-MB-231 cells reduced their ability to migrate in order to close the wound. Since we previously observed increased proliferation following Mnt depletion, we repeated these experiments following serum starvation of MDA-MB-231 cells. The analysis of these data showed the same results where MNT was essential for the migration capacity of TNBC cells.

Next, we evaluated the role of genes regulated by Mnt in EMT-related pathogenesis. Using DisGeNET (45), we searched for disease-associated SNPs in genes that were reexpressed following Mnt knockdown in our RNA-seq data. We found nine SNPs pertaining to five of these genes that are implicated in breast cancer (Table 1). These genes were *DIO1*, *NQO1*, *MUC1*, *PPARG*, *SCNN1A*, and *SFTPD*. The same SNP in *PPARG* was also implicated in liver fibrosis, while SNPs in *SCNN1A* and *SFTPD* were associated with cystic fibrosis. As important epithelial and transport genes, SNPs in *MUC1* and *SCNN1A* can hinder their normal functionality to promote EMT. Likewise, SNPs in *PPARG* can cause aberrant expression of detrimental genes due to its ubiquitous expression and widespread involvement in the regulation of energy storage (46). Given the important cellular roles of the above-described genes in immune function (*SFTPD*) and epithelial integrity (*MUC1*), for example, the suppressive effect of Mnt at these genes aligns with the GO analysis of genes upregulated following Mnt knockdown.

Overall, these data show that MNT is essential for cellular migration in primary EMT and aggressive breast cancer cells, and polymorphisms in MNT target genes occurs in other EMT-related pathologies.

MNT directly binds and represses epithelial genes via epigenetic mechanisms. Since MNT is a DNA binding protein, we were curious to understand if the gene expression changes could be linked to its DNA binding activity. Our earlier observations suggested that MNT is a repressor during EMT, as a much larger number of genes were transcriptionally derepressed upon MNT depletion during EMT, where they would otherwise be transcriptionally silenced (Fig. 2a). In order to identify key target genes regulated by MNT during EMT, we obtained existing MNT chromatin immunoprecipitation sequencing (ChIP-seq) data derived from HepG2 cells (47), which exhibit an epithelial-like morphology and undergo EMT when exposed to TGFβ (48). A comparison between MNT binding derived from ChIP-seq data and our transcriptome obtained upon Mnt knockdown revealed several genes that are potential direct targets of Mnt for transcriptional regulation (Fig. 4a). We chose a few of these genes for further functional analysis based on the following criteria: they increase in expression upon siMnt (consistent with the retention of epithelial characteristics), they decrease in expression during murine and human EMT (where epithelial cells acquire invasive mesenchymal properties), and they contain an E-box motif hallmark of bHLH occupancy. Visual inspection of these genes (*Aldoc*, *Arrb1*, *C1qtnf6*, *Cbs*, *Cln6*, *Gdp1l*, *Paics*, *Pgm2*, *Usp2*, *Usp46*, and *Zdhhc23*) in the MNT ChIP-seq data confirmed MNT occupancy at their promoter regions (Fig. 4b and Fig. S7a). We next attempted to validate this MNT occupancy in independent ChIP assays where we overexpressed GFP-tagged MNT during

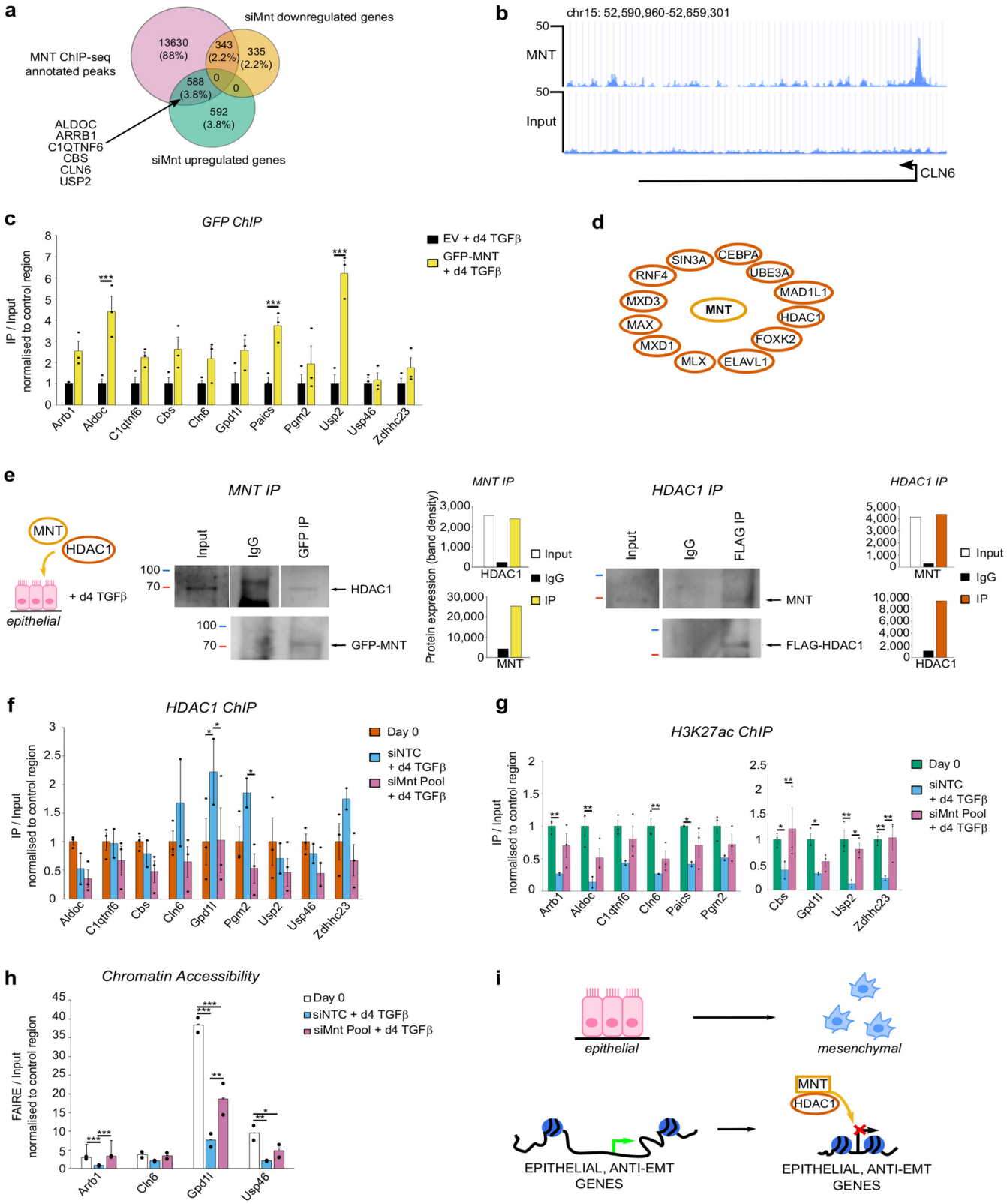

FIG 4 MNT directly binds and represses epithelial genes via epigenetic mechanisms. (a) A Venn diagram depicting overlapping genes between HepG2 MNT ChIP-seq (pink circle) and our siMnt transcriptome (downregulated, orange circle; upregulated, green circle). (b) UCSC genome browser screenshot showing enrichment of MNT at a representative target promoter in untreated HepG2 cells. The wiggle files were generated from four biological replicates. The gene is displayed as arrows representing the direction of transcription. The baseline on the *y* axis represents 0 values. (c) ChIP-qPCR results for GFP-tagged MNT (yellow bars) enrichment at Mnt target genes compared to empty vector control (EV; black bars) in NMuMG cells after 4 days of EMT and overexpression of

(Continued on next page)

EMT and performed ChIP using GFP-specific antibodies. Further qPCR analysis on these samples for selected targets showed MNT enrichment at the majority of these candidates (Fig. 4c), confirming that these genes are indeed MNT targets. As further validation, we performed ChIP-qPCR at a subset of these targets following depletion of Mnt, where we observed significant reductions in Mnt binding (i.e., enrichment) at these genes in siMnt versus siNTC (Fig. S7b). MNT contains a Sin3-interacting domain (SID) that is known to enable interaction with corepressive complexes containing Sin3A/Sin3B and histone deacetylases (HDACs) (49, 50). This is in line with our earlier observations, as we observed that MNT represses key epithelial/anti-EMT genes to promote EMT. We therefore analyzed known interaction partners of MNT and found HDAC1 among the 26 interactors reported on BioGRID (51) (Fig. 4d). To further substantiate these observations, we overexpressed GFP-MNT together with FLAG-HDAC1 during TGFβ-induced EMT (Fig. 4e, left) and performed immunoprecipitations for both proteins of interest. We successfully immunoprecipitated MNT (Fig. 4e, center) and HDAC1 (Fig. 4e, right) and pulled down HDAC1 and MNT in MNT and HDAC1 immunoprecipitations, respectively, confirming the association of MNT with repressive HDAC1 during EMT.

We next tested whether Mnt potentially recruits HDAC1 to its target genes to repress epithelial identity by performing a ChIP assay for HDAC1 following depletion of MNT during EMT. In line with our hypothesis, we observed significantly reduced enrichment of HDAC1 at several MNT target genes (Fig. 4f). Interestingly, HDAC1 enrichment increased during normal (siNTC) EMT at a few genes, while at other sites it was preenriched in untreated cells. This could be due to either earlier HDAC1 recruitment during TGFβ-induced EMT or known observations that HDAC1 is occasionally observed at active genes (52). Others have also shown that HAT/HDAC turnover is more important than HDAC1 enrichment alone in terms of regulating gene expression (53), especially given the number of transcriptional complexes (e.g., Sin3A/B, CoREST, NuRD, and MiDac) HDACs are involved in (54). Interestingly, overexpression of MNT during EMT also led to a tendency toward increased HDAC1 enrichment; however, this was only significant for one gene (Fig. S6g). This may be explained by poor binding enrichment of HDAC1, which others have also observed to be low but reproducible (52, 55, 56), resulting in a limited number of high-quality ChIP-seq data sets (47) for this well-known epigenetic modifier.

To confirm that MNT binding regulates the expression of its target genes via epigenetic remodeling, we subsequently performed ChIP assay for H3K27ac, the most widely used mark of active chromatin, and assessed chromatin accessibility via formaldehyde-associated isolation of regulatory elements (FAIRE) assay following Mnt depletion during EMT and analyzed these genes. In line with their expression kinetics, the promoters of these genes showed high levels of H3K27ac enrichment and chromatin accessibility in epithelial cells, which were both reduced upon induction of EMT (Fig. 4g and h and Fig. S6f). Interestingly, however, these genes fail to show such loss of H3K27ac, chromatin accessibility, and, consequently, gene expression when MNT was depleted during EMT. Further substantiating our findings, overexpression of MNT during EMT could reduce H3K27ac at MNT target promoters, albeit not significantly at all genes (Fig. S6h). This could be due to a sufficient reduction in the enrichment of this mark at these genes at day four of EMT, whereby no further reduction may be possible. Overall, these

FIG 4 Legend (Continued)
EV or GFP-MNT. (d) Network of direct MNT interactions, adapted from BioGRID4.4. (e) Schematic representation of the experimental procedure (left). Western blots of immunoprecipitated samples to validate MNT and HDAC1 interactions. NMuMG cells were cotransfected with GFP-MNT and FLAG-HDAC1, and anti-MNT (center) and HDAC1 (right) IPs were performed using GFP-trap agarose (GTA-10; Chromotek) for MNT or FLAG (F1804; Sigma-Aldrich) for HDAC1. Immunoblotting was performed to detect HDAC1 (sc-8410; Santa Cruz) and MNT (sc-376708; Santa Cruz) in MNT and HDAC1 precipitates (top). Successful IPs were confirmed by probing for GFP or FLAG (bottom). (f) ChIP-qPCR results for HDAC1 enrichment at Mnt target genes in untreated NMuMG cells (day 0) or NMuMG cells after 4 days of EMT with nontargeting control (siNTC) or siRNA-mediated knockdown of Mnt (siMnt). (g) ChIP-qPCR results for H3K27ac enrichment at Mnt target genes in untreated NMuMG cells (day 0) or NMuMG cells after 4 days of EMT with nontargeting control (siNTC) or siRNA-mediated knockdown of Mnt (siMnt). (h) Chromatin accessibility was determined by FAIRE qPCR at Mnt target genes in untreated NMuMG cells (day 0) or NMuMG after 4 days of EMT with nontargeting siRNA (siNTC) or siRNA-mediated knockdown of Mnt (siMnt). (i) Schematic depiction of how MNT functions to promote EMT. Error bars represent the means ± SEM from three independent biological replicates ($n = 3$). *, $P < 0.05$; **, $P < 0.01$; ***, $P < 0.001$; Student's unpaired two-tailed t test (c), two-way (f and h), or one-way (g) ANOVA with Bonferroni multiple-comparison test, alpha = 0.05.

data show that MNT regulates phenotypic and molecular changes underlying EMT via epigenetic repression of its target epithelial genes (Fig. 4i).

DISCUSSION

EMT has been classified into specific subtypes; however, the core mechanisms of this process across developmental EMT, wound healing/fibrotic EMT, and cancer-related EMT appear to be highly conserved (57). Therefore, understanding mechanisms underlying EMT will have wider implications not only for relevant developmental processes and wound healing but also for various EMT-related pathological conditions, including cancer metastasis, organ fibrosis (58), diabetic complications (59, 60), heart disease (61), and immunocompromising conditions like cystic fibrosis (62).

While a few bHLH TFs such as TWIST1 and TWIST2 have been established for their role in EMT, no comprehensive study has investigated the kinetics and potential function of many other bHLH TFs during EMT. We therefore sought to identify bHLH TFs that were potentially required for EMT progression. Using transcriptome data from various stages of mammary EMT in mouse and human cells, we identified various categories of bHLH TFs that showed distinct expression kinetics during EMT. A functional siRNA screen identified Mnt as a novel and potent regulator of molecular and morphological changes during mammary EMT, owing to its induction and sustained expression at the onset of and throughout EMT. During this screen, we also found six bHLH candidates that decreased during EMT and were found to promote epithelial identity *in vitro* rather than promote EMT. This is in line with the published data on these candidates in other candidates, e.g., Tcfec was shown to be highly induced in E16.5 intestinal epithelium (63), and Mxd3 regulated absorptive intestinal epithelial cell commitment (64). When Mnt was depleted following induction of EMT, cells failed to gain mesenchymal markers such as fibronectin and retained epithelial markers, e.g., E-cadherin and ZO1. Furthermore, focal adhesions, cytoskeletal remodeling, and cellular size were characteristically closer to epithelial cells upon Mnt knockdown. The potency of MNT during EMT was further substantiated by our findings that MNT was able to significantly accelerate ongoing TGFβ-induced EMT.

The defects in EMT following Mnt depletion were not limited to a few cellular markers but were widespread, as observed in the massive transcriptional reprogramming that occurred following Mnt knockdown, despite the presence of the strong EMT inducer TGFβ. Gene ontology analysis of genes upregulated upon Mnt knockdown revealed epithelial cell-related processes, cell adhesion, cell shape/growth regulation, and apoptosis, indicative of a well-controlled cellular environment that promotes epithelial cell identity. In addition, metabolic (such as lipid metabolism but also carbohydrate and lactate metabolism) and enzymatic (e.g., oxidation-reduction) processes were associated with genes repressed by Mnt. Self-sufficiency and altered metabolism are well-known hallmarks of cancer cells (3, 65). Hence, Mnt may further facilitate cancer progression by altering cell metabolism as well as promoting aberrant EMT. The genes downregulated upon Mnt knockdown during EMT included those involved in migration and actin filament and cytoskeletal organization. It is important to mention that given the design of these experiments, we would miss gene interactions of Mnt at the very early stage of EMT, if any.

As EMT is involved in developmental and pathological processes, we chose well-known breast cancer cell lines and cohorts for validation. We observed higher MNT expression in cell lines that reflect TNBC versus luminal and HER2$^+$ subtypes, which indicates that high MNT expression is associated with this aggressive molecular subtype of breast cancer. Depletion of MNT in TNBC cells significantly inhibited wound closure in a scratch assay. This effect, which was not due to altered proliferation as assessed by serum starvation, indicates that MNT is needed for their migration. This observation agrees with previous reports whereby loss of MNT is associated with Miller-Dieker syndrome (lissencephaly) due to defects in neuronal migration (66, 67). When we reclassified the TCGA-BRCA cohort according to the EMT status of the tumor, we saw significantly higher MNT expression in EMT-High tumors versus EMT Low, and as Mnt is a repressor, we observed opposing behavior in the expression of its target genes in these tumors. Multiple alterations in MNT are reported in

invasive breast cancer and glioma, and cases with altered MNT tended to have increased morbidity and fewer disease/progression-free months (68, 69). This may also be applicable to other cancers where EMT is aberrantly activated, such as ovarian and gastric.

Interestingly, the Mnt-repressed genes also appeared to be targets of NFE2L2 and HNF4A, which are known to repress the well-known EMT-inducing TF Snail (44, 70). Furthermore, genes downregulated following Mnt knockdown (i.e., upregulated during normal EMT) were enriched for motifs of known EMT inducers such as FOSL2, SMAD4, MYC, TCF3, and EGR1 (27, 41–43). The opposing enrichment of MNT (genes repressed during EMT) and MYC (genes upregulated during EMT) is in line with previous observations where Mnt-deficient murine fibroblasts and mammary tissue exhibited characteristics of Myc-overexpressing cells (71, 72). Overall, these observations suggest that the Mnt-governed gene regulatory program interacts with the core EMT program, which is controlled by other key TFs, hence MNT is central to the molecular circuitry underlying EMT.

We also identified a number of SNPs within genes repressed by MNT during EMT that have been implicated in EMT-mediated breast carcinoma, liver fibrosis, or cystic fibrosis. The involvement of EMT in cystic fibrosis is not surprising given its role in asthma, COPD, and idiopathic pulmonary fibrosis (62). SNPs were found within *DIO1*, *NQO1*, *MUC1*, *PPARG*, *SCNN1A*, *SFTPD*, and *NQO1* (Table 1). These genes are involved in thyroid hormone activation (73) (*DIO1*), protective mucous barrier formation on epithelial surfaces (74) (*MUC1*), regulation of adipocyte differentiation (75) (as well as cancer [76] and diabetes [77] pathology; *PPARG*), fluid and electrolyte transport across epithelia (78) (*SCNN1A*), quinone reduction (79) (*NQO1*), and pulmonary defense against inhaled microorganisms and chemicals (80) (*SFTPD*). Important epithelial and transport genes SNPs in *MUC1* and *SCNN1A* can hinder their normal functionality to promote EMT. For example, NF-κB-mediated increases in MUC1 are detected in abnormally high levels in the mucus of cystic fibrosis patients, creating an ideal environment for bacteria to grow (81). Likewise, SNPs in *PPARG* and *DIO1* can cause aberrant expression of detrimental EMT-promoting genes. Given the important cellular roles of these genes in immune function, metabolism, and epithelial integrity, the suppressive effect of Mnt at these genes aligns with our derived GO analysis of genes upregulated following Mnt depletion during EMT. Overall, these data suggest that MNT and its target genes have a role in other pathological conditions associated with EMT.

As a member of the Mad family within the bHLH TF family (31), MNT, like other bHLH TFs, binds to specific E-box motifs CACGTG/CATGTTG, while other family members, such as TWIST and MYOD, bind CAGCTG/CACCTG (24). We find that MNT is induced and directly binds at the promoters of many epithelial identity genes during EMT and recruits HDAC1 to these target loci. This is followed by massive epigenetic remodeling at target loci, as shown by loss of H3K27ac enrichment and chromatin accessibility, ultimately leading to repression of these epithelial genes and progression of the cells toward the mesenchymal fate. In addition to its interaction with HDAC1, MNT potentially interacts with the E3 ubiquitin ligase RNF4, which tags PIAS1 for degradation (82). PIAS1 normally SUMOylates BRCA1-BARD1 dimers following DNA damage (82) and suppresses TGFβ-induced invasive growth (EMT) of breast cancer-derived organoids through SUMOylation of SnoN (83). Perhaps RNF4 protects Mnt from PIAS1-mediated degradation and prevents the suppressive effect of PIAS1 on EMT. Mnt was also putatively identified as a Sox4 target (84), and both Sox4 and Mnt were implicated in a TF-microRNA network underlying EMT (85). These interactions warrant future investigation for their occurrence and relevance during EMT. Moreover, since bHLH factors generally function as homodimers or heterodimers, future studies should investigate how MNT functions during EMT. In addition, it will be exciting to reveal genetic and epigenetic mechanisms that guide the targeting of MNT to specific loci during EMT. Overall, our observations establish MNT as a novel essential regulator of EMT in mammary epithelial cells and provide knowledge of the wider relevance from basic to translational research.

MATERIALS AND METHODS

Cell culture. A subclone of mouse mammary gland (NMuMG/E9) cells has been described previously (94) and was grown in Dulbecco's modified essential medium (DMEM) supplemented with 10% fetal bovine

serum (FBS), 2 mM GlutaMAX, and 1× MEM nonessential amino acids at 37°C with 7% CO_2 in a humid incubator. Cells were routinely tested for mycoplasma contamination. HMLE cells, a kind gift from Robert Weinberg, were cultured in Lonza primary cell culture medium. MDA-MB-231 cells were grown in DMEM supplemented with 10% FBS. For TGFβ time course experiments, NMuMG cells and HMLE cells were treated with 2 ng/ml or five ng/ml TGFβ (240-B/CF; R&D Systems), respectively, for up to 4 days. The medium was changed to fresh media containing TGFβ on day two.

siRNA-mediated knockdown. For siRNA-mediated knockdown experiments, NMuMG cells were seeded at the same starting density and transfected every second day with 20 pmol (for a 6-well plate, scaled up or down as appropriate) ON-TARGET plus mouse Mnt SMART pool siRNA (L-058469-010005 [Dharmacon], which contains the following four Mnt-targeting siRNAs: CUCCAGAUCUAGUGCCGAA, GGACAACGUUGACGAGGAG, UUGAGACCCUGAAGCGCAA, and GCAACAACAGAGAGCACGU) or individual Mnt-targeting siRNAs (IF only) and Lipofectamine RNAiMAX (13778-150; Invitrogen) according to the manufacturer's instructions. For experiments during TGFβ-induced EMT, TGFβ induction was performed at the same time that siRNA was added to avoid indirect effects due to loss of protein function.

Plasmid-mediated overexpression. NMuMG cells were seeded at the same starting density, treated with TGFβ, and transfected with 5 μg (for 6-well plates; scaled up or down as appropriate) of GFP-MNT construct (EX-P0106-Lv103; kindly provided by J. León, Madrid) with/without FLAG-HDAC1 (plasmid 13820; Addgene) using Lipofectamine 2000 (11668019; Invitrogen) according to the manufacturer's instructions. The GFP-MNT construct expresses human MNT (NM_020310) under the control of the cytomegalovirus (CMV) promoter and contains an N-terminal GFP tag. The FLAG-HDAC1 construct expresses human HDAC1 (NM_004964) under the control of the CMV promoter and contains a C-terminal FLAG tag. Plasmid integrity was confirmed via DNA sequencing (TubeSeq; Eurofins) using the following primers: GFP-MNT, CCGACAACCACTACCTGA and ATTGTGGATGAATACTGCC; FLAG-HDAC1, TAATACGACTCACTATAGGG and TAGAAGGCACAGTCGAGG.

Immunofluorescence. NMuMG cells were seeded on coverslips 16 h before siRNA transfection and TGFβ treatment. Cells were retransfected on day two and harvested on day four. All knockdown treatments were performed in parallel. Cells were subsequently fixed with 4% paraformaldehyde in phosphate-buffered saline (PBS) for 15 min at room temperature and permeabilized with 0.2% Triton X-100 in PBS for 15 min. Subsequently, the cells were blocked with 5% FBS, 1% goat serum, and 2% bovine serum albumin (BSA) in PBS for 30 min at room temperature and were incubated with ZO-1 (617300, 1:100; Life Technologies) at 4°C overnight. The cells were then washed with PBS and incubated with fluorochrome-conjugated secondary antibody (donkey anti-rabbit AF568 [A10042; Thermo Fisher Scientific], 1:500) or Phalloidin-633 [A22284, 1:200; Life Technologies] for 1 h at room temperature. The coverslips were counterstained with Hoechst (20 mM 33342 solution; 62249; Thermo Fisher Scientific), mounted with Vectashield Hardset mounting medium (Vector Laboratories), and imaged using a confocal laser scanning SP5 microscope. For each stain, exposures were defined using the untreated control, and these settings were maintained for all treatment groups. Three-dimensional deconvolution was performed, and scale bars were added using LASX software (Leica Microsystems, UK).

SI calculation. Spindle indices (SI) of individual cells were calculated from at least 40 cells from a minimum of three 40× images per treatment from the same experiment (for IF) or three independent experiments (for bright field). The length and width of all cells were measured using Image J software, U.S. National Institutes of Health, Bethesda, MD, USA. No cells were excluded from this quantification. The method was adopted from Koo et al. (35), whereby the SI was calculated as the ratio of length (l) to width (w), i.e., SI = l/w of each cell. An example of how this was performed can be found in Fig. 3b.

Wounding migration assay. MDA-MB-231 cells were seeded at equal densities, and following siRNA treatment, a scratch wound was generated using a 10-μl pipette tip on confluent cell monolayers growing in 6-well or 12-well culture plates. Cells were then washed with fresh medium to remove floating cells. Bright-field images were taken at ×10 magnification immediately after the wound was inflicted and 24 h later. The wound area was quantified using ImageJ software.

Apoptosis assay. To induce apoptosis, medium was removed from all wells prior to UV irradiation, and transfected (siNTC or siMnt) NMuMG cells were exposed to 100 J/m^2 of UV in the UVP Trans Linker CL-1000 shortwave crosslinker. Medium was then replenished, and cells were returned to the incubator for 1 h. The apoptosis assay was performed thereafter, using an allophycocyanin annexin V antibody according to the manufacturer's instructions (550474; BD Biosciences). Briefly, cells were trypsinized as normal and the pellets were washed twice with PBS. Each treatment was split into two pellets, one for unstained control and one for annexin V. Pellets were treated with DNase I (BD Biosciences) for 15 min at room temperature to reduce cellular aggregation. The pellets were subsequently washed with Hanks' balanced salt solution (HBSS) plus $MgCl_2$, and unstained control pellets were resuspended in this solution. For annexin V staining, pellets were resuspended in annexin binding buffer (HBSS plus $MgCl_2$ plus HEPES [pH 7.5], plus NaCl plus $CaCl_2$) and incubated with annexin V for 15 min at room temperature in the dark. Pellets were subsequently washed and resuspended in annexin binding buffer. Cells were then analyzed on a FACSCanto II flow cytometer using DIVA software.

Immunoblotting. NMuMG cells were lysed in radioimmunoprecipitation assay buffer, and protein concentrations were quantified using Bradford reagent. Equal amounts of protein (30 μg) were boiled in 5× SDS-PAGE loading buffer, subjected to polyacrylamide gel electrophoresis, transferred to a polyvinylidene difluoride (PVDF) membrane, and probed overnight at 4°C with the appropriate primary antibody, Mnt (A303-627A-T, 1:100, Bethyl Laboratories; sc-376708, 1:100, Santa Cruz; GTX105467, 1:500, GeneTex; or ABP51810, 1:500, Abbkine), E-cadherin (610182, 1:1,000; BD Biosciences); fibronectin (F3648, 1:500; Sigma-Aldrich), HDAC1 (sc-8410, 1:200; Santa Cruz), β-actin (sc-47778, 1:1,000; Santa Cruz), and glyceraldehyde-3-phosphate dehydrogenase (GAPDH) (sc-47724, 1:1,000, Santa Cruz), and secondary antibodies.

Immunoprecipitation. NMuMG cells were treated with TGFβ and cotransfected with 5 μg of each GFP-tagged MNT and FLAG-tagged HDAC1 construct using Lipofectamine 2000 (11668019; Invitrogen). Cells were retransfected on day two and harvested on day four. Cells were lysed in lysis buffer (50 mM HEPES [pH 7.5], 150 mM NaCl, 5 mM EGTA, 1.5 mM $MgCl_2$, 1% glycerol, 1% Triton X-100) and incubated on ice for 30 min before sonication (3 cycles of 30 s on/40 s off). Protein concentration was measured by Bradford assay and adjusted to 2 mg/ml, and 10% was taken as the input. Proteins were immunoprecipitated overnight at 4°C with 5 μg of the appropriate antibody, GFP-trap agarose (GTA-10; Chromotek) for MNT or FLAG (F1804; Sigma-Aldrich) for HDAC1. Lysates were also incubated with rabbit or mouse IgG as controls as appropriate. Protein G beads were added to lysates and incubated for 3 h at 4°C. The bound beads were washed three times with wash buffer (50 mM Tris-HCl [pH 7.5], 150 mM NaCl, 5 mM EDTA, 0.1% Triton X-100), eluted in 1× Laemmli buffer, and analyzed by immunoblotting. For all IP experiments, immunoprecipitated material was eluted with an equal volume of elution buffer, and the same volume of samples was loaded on the gel for immunoblot analysis, using the same HDAC1 and MNT (sc-376708, Santa Cruz, 1:100) antibodies described above. Successful IPs were confirmed by probing for GFP (sc-9996, 1:200; Santa Cruz) or FLAG (F1804, 1:1,000; Sigma-Aldrich).

RNA-seq. Total RNA was prepared using TRIzol (Invitrogen) from three biological replicates, each of siNTC and siMnt NMuMG cells during day 4 TGFβ treatment. Library preparation using the Ovation SoLo RNA-seq kit (Tecan Genomics) was performed according to the manufacturer's instructions. RNA-seq libraries for all six samples were generated using the Illumina NextSeq kit. Single-end sequencing with a sequencing depth of 50 million reads was requested, resulting in 75-bp reads. The reads were aligned to the mouse genome (mm9) using TopHat (86) (version 2.1.0) with the default options. After library size normalization using DESeq (87) (version 3.5), expression was quantified and differential expression analysis was performed using the DESeq package (87). Gene set enrichment analysis for biological processes was performed using DAVID (88, 89) with a P value of <0.05.

ChIP assay. NMuMG cells were cross-linked in a medium containing 1% formaldehyde for 10 min at room temperature, neutralized with 0.125 M glycine, rinsed twice with PBS, and scraped before centrifugation at 600 × g for 7 min. The pellets were suspended in buffer L1 (50 mM HEPES KOH [pH 7.5], 140 mM NaCl, 1 mM EDTA [pH 8.0], 10% glycerol, 5% NP-40, and 0.25% Triton X-100) and incubated for 10 min at 4°C. The cells were then suspended in buffer L2 (200 mM NaCl, 1 mM EDTA [pH 8.0], 0.5 mM EGTA [pH 8.0], 10 mM Tris [pH 8.0]) for 10 min at room temperature. Finally, the pellet was suspended in buffer L3 (1 mM EDTA [pH 8.0], 0.5 mM EGTA [pH 8.0], 10 mM Tris [pH 8.0], 100 mM NaCl, 0.1% Na-deoxycholate, 0.17 mM sodium lauroyl sarcosine) containing protease inhibitors and was incubated at 4°C overnight following sonication using Bioruptor plus (Diagenode). Sixty micrograms of chromatin was incubated overnight at 4°C with 2 μg of the antibody targeting H3K27ac (ab4729; Abcam) or 5 μg of the following antibodies: HDAC1 (ab7028; Abcam), FLAG (F1804; Sigma-Aldrich), GFP (A11122; Thermo Fisher Scientific), and MNT (sc-376708; Santa Cruz). Samples were then incubated with preblocked beads for 3 h. The beads were washed twice with L3 and once with 1 ml of DOC buffer (10 mM Tris [pH 8.0], 0.25 M LiCl, 0.5% NP-40, 0.5% deoxycholate, 1 mM EDTA), and the bound chromatin was eluted in 1% SDS–0.1 M $NaHCO_3$. Chromatin was subsequently treated with RNase A (0.2 mg/ml) for 30 min at 37°C. Crosslinking was reversed with proteinase K (50 μg/ml) for 2.5 h at 55°C, followed by 65°C overnight with gentle shaking. The DNA was purified by phenol-chloroform-isoamyl extraction followed by ethanol precipitation and was recovered in TE buffer. Real-time qPCR on this ChIP material was performed using SYBR green and ChIP (1:40) or input (1:100) DNA per reaction. A list of primers used can be found in Table S5 in the supplemental material.

External data sets. For RNA-seq data analysis we used The Cancer Genome Atlas (TCGA) Research Network (https://www.cancer.gov/tcga) breast cancer (TCGA-BRCA) transcriptome data. We recognize the contribution of the breast cancer donors and the work performed by the research groups involved. The HT-seq count files of 1,102 patients were retrieved from the TCGA database using the GDC Data Transfer Tool Client. Gene expression counts were normalized using the variance stabilizing transformation (VST) method. Of the 1,102 patients in this cohort, 809 patients had molecular subtype information available: $n = 411$ luminal A patients, $n = 174$ luminal B, $n = 65$ $HER2^+$, $n = 134$ TNBC, and $n = 25$ classed as normal.

The MNT ChIP-seq data set of the HepG2 cell line (Snyder laboratory, Stanford) was obtained from the European Nucleotide Archive (ENA) under study number PRJNA63443 (https://www.ebi.ac.uk/ena/data/view/PRJNA63443). Quality control was performed on four biological replicates using FASTQC (http://www.bioinformatics.babraham.ac.uk/projects/fastqc), and trimmed reads (TrimGalore; https://github.com/FelixKrueger/TrimGalore) were aligned to the human hg19 genome using Bowtie2 (90). Each read was aligned to maximally one position in the genome. SAMTOOLS was used to convert the SAM file into BAM format and to sort and index the BAM file. The peaks were called using MACS2 (91) using default parameters. WIG files were generated using the QuasR (92) package and visualized using the UCSC genome browser. The raw read counts that aligned to each genomic feature (promoters, peaks, and enhancers) were calculated and normalized using QuasR. HOMER v4.7 (93) was used to annotate the peaks.

Identification of EMT-High and EMT-Low tumor groups in the TCGA-BRCA cohort. The TCGA-BRCA mRNA expression z-scores of breast cancer tumors ($n = 1,102$) were obtained from cBioPortal (68, 69) using the cgdsr R package (version 1.3.0) (95). The Spearman correlation for seven mesenchymal markers (ZEB1, ZEB2, TWIST2, SNAI2, FN1, QKI, and RBFOX2) and five epithelial marker genes (OVOL1, OVOL2, ESRP1, ESRP2, and CLDN3) were calculated using the corrplot R package (version 0.84) (96) with a significant coefficient (95% confidence level; $P < 0.05$) to select only those markers that separated patients with greater distinction. The EMT scores were calculated for each sample by subtracting the average expression z-scores of the 5 epithelial markers from the average expression z-scores of the 7 mesenchymal markers. The tumor samples were then classified as EMT High (defined by EMT scores ≥

highest 1/3) and EMT Low (defined by EMT scores ≤ lowest 1/3) based on the calculated EMT scores (97). The Pheatmap R package (version 1.0.12) (98) was used to construct the heatmap of expression levels of the 12 markers in the EMT-High and EMT-Low groups defined above. To increase the confidence in our downstream analysis, we used a stringent approach and only selected the top 25% of tumors from each EMT-High and EMT-Low group. This ultimately resulted in $n = 76$ ($301 \times 0.25 = 76$) EMT-High and $n = 144$ EMT-Low ($578 \times 0.25 = 144$) tumors.

Statistics and reproducibility. All experiments were performed in biological triplicates unless otherwise specified. Data are expressed as means ± the standard error of the means (means ± SEM). Statistical analysis was performed with GraphPad Prism software, version 5.01 (GraphPad Software Inc.). Significant differences were identified using Student's unpaired two-tailed *t* test with 95% confidence interval (for $n = 2$ groups) or analysis of variance (ANOVA) with Bonferroni's multiple-comparison test (for $n \geq 3$ groups). Alpha = 0.05. A *P* value of <0.05 was considered statistically significant.

Data availability. The next-generation sequencing data generated in this study have been submitted to the NCBI Gene Expression Omnibus (GEO; http://www.ncbi.nlm.nih.gov/geo/) under accession number GSE158546.

SUPPLEMENTAL MATERIAL

Supplemental material is available online only.

SUPPLEMENTAL FILE 1, PDF file, 2.6 MB.
SUPPLEMENTAL FILE 2, PDF file, 0.6 MB.
SUPPLEMENTAL FILE 3, PDF file, 1.1 MB.
SUPPLEMENTAL FILE 4, PDF file, 1.3 MB.
SUPPLEMENTAL FILE 5, PDF file, 1.1 MB.
SUPPLEMENTAL FILE 6, PDF file, 9.9 MB.
SUPPLEMENTAL FILE 7, PDF file, 0.2 MB.
SUPPLEMENTAL FILE 8, XLSX file, 0.04 MB.
SUPPLEMENTAL FILE 9, PDF file, 0.3 MB.

ACKNOWLEDGMENTS

We thank the members of the Tiwari lab for their cooperation and critical feedback throughout this study. The support from the Core Facilities of the WWIEM (QUB) and IMB (Mainz) is gratefully acknowledged, especially the microscopy, cytometry, and genomics core facilities.

D.P.L. performed computational analysis, analyzed data, and wrote the manuscript. L.A. performed experiments and analyzed data. M.I. provided bioinformatics tools and performed computational analysis. V.K.T. designed the study, analyzed data, and wrote the manuscript. All authors read and approved the final manuscript.

We have no competing interests to declare.

REFERENCES

1. Georgakopoulos-Soares I, Chartoumpekis DV, Kyriazopoulou V, Zaravinos A. 2020. EMT factors and metabolic pathways in cancer. Front Oncol 10:499. https://doi.org/10.3389/fonc.2020.00499.
2. Yang J, Antin P, Berx G, Blanpain C, Brabletz T, Bronner M, Campbell K, Cano A, Casanova J, Christofori G, Dedhar S, Derynck R, Ford HL, Fuxe J, García de Herreros A, Goodall GJ, Hadjantonakis A-K, Huang RJY, Kalcheim C, Kalluri R, Kang Y, Khew-Goodall Y, Levine H, Liu J, Longmore GD, Mani SA, Massagué J, Mayor R, McClay D, Mostov KE, Newgreen DF, Nieto MA, Puisieux A, Runyan R, Savagner P, Stanger B, Stemmler MP, Takahashi Y, Takeichi M, Theveneau E, Thiery JP, Thompson EW, Weinberg RA, Williams ED, Xing J, Zhou BP, Sheng G, on behalf of the EMTIA. 2020. Guidelines and definitions for research on epithelial–mesenchymal transition. Nat Rev Mol Cell Biol 21:341–352. https://doi.org/10.1038/s41580-020-0237-9.
3. Burger GA, Danen EHJ, Beltman JB. 2017. Deciphering epithelial-mesenchymal transition regulatory networks in cancer through computational approaches. Front Oncol 7:162–162. https://doi.org/10.3389/fonc.2017.00162.
4. Bakir B, Chiarella AM, Pitarresi JR, Rustgi AK. 2020. EMT, MET, plasticity, and tumor metastasis. Trends Cell Biol 30:764–776. https://doi.org/10.1016/j.tcb.2020.07.003.
5. Sims AH, Howell A, Howell SJ, Clarke RB. 2007. Origins of breast cancer subtypes and therapeutic implications. Nat Clin Pract Oncol 4:516–525. https://doi.org/10.1038/ncponc0908.
6. Herschkowitz JI, Zhao W, Zhang M, Usary J, Murrow G, Edwards D, Knezevic J, Greene SB, Darr D, Troester MA, Hilsenbeck SG, Medina D, Perou CM, Rosen JM. 2012. Comparative oncogenomics identifies breast tumors enriched in functional tumor-initiating cells. Proc Natl Acad Sci U S A 109:2778–2783. https://doi.org/10.1073/pnas.1018862108.
7. Eroles P, Bosch A, Pérez-Fidalgo JA, Lluch A. 2012. Molecular biology in breast cancer: intrinsic subtypes and signaling pathways. Cancer Treat Rev 38:698–707. https://doi.org/10.1016/j.ctrv.2011.11.005.
8. Su Y, Hopfinger NR, Nguyen TD, Pogash TJ, Santucci-Pereira J, Russo J. 2018. Epigenetic reprogramming of epithelial mesenchymal transition in triple negative breast cancer cells with DNA methyltransferase and histone deacetylase inhibitors. J Exp Clin Cancer Res 37:314–314. https://doi.org/10.1186/s13046-018-0988-8.
9. Tan TZ, Miow QH, Miki Y, Noda T, Mori S, Huang RY-J, Thiery JP. 2014. Epithelial-mesenchymal transition spectrum quantification and its efficacy in deciphering survival and drug responses of cancer patients. EMBO Mol Med 6:1279–1293. https://doi.org/10.15252/emmm.201404208.
10. Wang Y, Zhou BP. 2011. Epithelial-mesenchymal transition in breast cancer progression and metastasis. Chin J Cancer 30:603–611. https://doi.org/10.5732/cjc.011.10226.
11. Tiwari N, Gheldof A, Tatari M, Christofori G. 2012. EMT as the ultimate survival mechanism of cancer cells. Semin Cancer Biol 22:194–207. https://doi.org/10.1016/j.semcancer.2012.02.013.

12. Taube JH, Herschkowitz JI, Komurov K, Zhou AY, Gupta S, Yang J, Hartwell K, Onder TT, Gupta PB, Evans KW, Hollier BG, Ram PT, Lander ES, Rosen JM, Weinberg RA, Mani SA. 2010. Core epithelial-to-mesenchymal transition interactome gene-expression signature is associated with claudin-low and metaplastic breast cancer subtypes. Proc Natl Acad Sci U S A 107:15449–15454. https://doi.org/10.1073/pnas.1004900107.
13. Navandar M, Garding A, Sahu SK, Pataskar A, Schick S, Tiwari VK. 2017. ERK signaling modulates epigenome to drive epithelial to mesenchymal transition. Oncotarget 8:29269–29281. https://doi.org/10.18632/oncotarget.16493.
14. Sahu SK, Tiwari N, Pataskar A, Zhuang Y, Borisova M, Diken M, Strand S, Beli P, Tiwari VK. 2017. FBXO32 promotes microenvironment underlying epithelial-mesenchymal transition via CtBP1 during tumor metastasis and brain development. Nat Commun 8:1523. https://doi.org/10.1038/s41467-017-01366-x.
15. Sahu SK, Garding A, Tiwari N, Thakurela S, Toedling J, Gebhard S, Ortega F, Schmarowski N, Berninger B, Nitsch R, Schmidt M, Tiwari VK. 2015. JNK-dependent gene regulatory circuitry governs mesenchymal fate. EMBO J 34:2162–2181. https://doi.org/10.15252/embj.201490693.
16. Morel AP, Hinkal GW, Thomas C, Fauvet F, Courtois-Cox S, Wierinckx A, Devouassoux-Shisheboran M, Treilleux I, Tissier A, Gras B, Pourchet J, Puisieux I, Browne GJ, Spicer DB, Lachuer J, Ansieau S, Puisieux A. 2012. EMT inducers catalyze malignant transformation of mammary epithelial cells and drive tumorigenesis toward claudin-low tumors in transgenic mice. PLoS Genet 8:e1002723. https://doi.org/10.1371/journal.pgen.1002723.
17. Ding S, Zhang W, Xu Z, Xing C, Xie H, Guo H, Chen K, Song P, Gu Y, Xiao F, Zhou L, Zheng S. 2013. Induction of an EMT-like transformation and MET in vitro. J Transl Med 11:164. https://doi.org/10.1186/1479-5876-11-164.
18. Uretmen Kagiali ZC, Sanal E, Karayel Ö, Polat AN, Saatci Ö, Ersan PG, Trappe K, Renard BY, Önder TT, Tuncbag N, Şahin Ö, Ozlu N. 2019. Systems-level analysis reveals multiple modulators of epithelial-mesenchymal transition and identifies DNAJB4 and CD81 as novel metastasis inducers in breast cancer. Mol Cell Proteomics 18:1756–1771. https://doi.org/10.1074/mcp.RA119.001446.
19. Tiwari N, Tiwari VK, Waldmeier L, Balwierz PJ, Arnold P, Pachkov M, Meyer-Schaller N, Schubeler D, van Nimwegen E, Christofori G. 2013. Sox4 is a master regulator of epithelial-mesenchymal transition by controlling Ezh2 expression and epigenetic reprogramming. Cancer Cell 23:768–783. https://doi.org/10.1016/j.ccr.2013.04.020.
20. Pataskar A, Jung J, Smialowski P, Noack F, Calegari F, Straub T, Tiwari VK. 2016. NeuroD1 reprograms chromatin and transcription factor landscapes to induce the neuronal program. EMBO J 35:24–45. https://doi.org/10.15252/embj.201591206.
21. Sun L, Fang J. 2016. Epigenetic regulation of epithelial-mesenchymal transition. Cell Mol Life Sci 73:4493–4515. https://doi.org/10.1007/s00018-016-2303-1.
22. Lamouille S, Xu J, Derynck R. 2014. Molecular mechanisms of epithelial-mesenchymal transition. Nat Rev Mol Cell Biol 15:178–196. https://doi.org/10.1038/nrm3758.
23. Iwafuchi-Doi M, Zaret KS. 2014. Pioneer transcription factors in cell reprogramming. Genes Dev 28:2679–2692. https://doi.org/10.1101/gad.253443.114.
24. Jones S. 2004. An overview of the basic helix-loop-helix proteins. Genome Biol 5:226. https://doi.org/10.1186/gb-2004-5-6-226.
25. Gallo C, Fragliasso V, Donati B, Torricelli F, Tameni A, Piana S, Ciarrocchi A. 2018. The bHLH transcription factor DEC1 promotes thyroid cancer aggressiveness by the interplay with NOTCH1. Cell Death Dis 9:871. https://doi.org/10.1038/s41419-018-0933-y.
26. Huilgol D, Venkataramani P, Nandi S, Bhattacharjee S. 2019. Transcription factors that govern development and disease: an Achilles heel in cancer. Genes 10:794. https://doi.org/10.3390/genes10100794.
27. Peinado H, Olmeda D, Cano A. 2007. Snail, Zeb and bHLH factors in tumor progression: an alliance against the epithelial phenotype? Nat Rev Cancer 7:415–428. https://doi.org/10.1038/nrc2131.
28. Tarczewska A, Greb-Markiewicz B. 2019. The significance of the intrinsically disordered regions for the functions of the bHLH transcription factors. Int J Molecular Sciences 20:5306. https://doi.org/10.3390/ijms20215306.
29. Bedi U, Mishra VK, Wasilewski D, Scheel C, Johnsen SA. 2014. Epigenetic plasticity: a central regulator of epithelial-to-mesenchymal transition in cancer. Oncotarget 5:2016–2029. https://doi.org/10.18632/oncotarget.1875.
30. Weber D, Wiese C, Gessler M. 2014. Hey bHLH transcription factors. Curr Top Dev Biol 110:285–315. https://doi.org/10.1016/B978-0-12-405943-6.00008-7.
31. Meroni G, Reymond A, Alcalay M, Borsani G, Tanigami A, Tonlorenzi R, Lo Nigro C, Messali S, Zollo M, Ledbetter DH, Brent R, Ballabio A, Carrozzo R. 1997. Rox, a novel bHLHZip protein expressed in quiescent cells that heterodimerizes with Max, binds a non-canonical E box and acts as a transcriptional repressor. EMBO J 16:2892–2906. https://doi.org/10.1093/emboj/16.10.2892.
32. Skinner MK, Rawls A, Wilson-Rawls J, Roalson EH. 2010. Basic helix-loop-helix transcription factor gene family phylogenetics and nomenclature. Differentiation 80:1–8. https://doi.org/10.1016/j.diff.2010.02.003.
33. Khan S, Stott SRW, Chabrat A, Truckenbrodt AM, Spencer-Dene B, Nave K-A, Guillemot F, Levesque M, Ang S-L. 2017. Survival of a novel subset of midbrain dopaminergic neurons projecting to the lateral septum is dependent on NeuroD proteins. J Neurosci 37:2305–2316. https://doi.org/10.1523/JNEUROSCI.2414-16.2016.
34. Uittenbogaard M, Baxter KK, Chiaramello A. 2010. NeuroD6 genomic signature bridging neuronal differentiation to survival via the molecular chaperone network. J Neurosci Res 88:33–54. https://doi.org/10.1002/jnr.22182.
35. Koo V, El Mekabaty A, Hamilton P, Maxwell P, Sharaf O, Diamond J, Watson J, Williamson K. 2010. Novel in vitro assays for the characterization of EMT in tumourigenesis. Cell Oncol 32:67–76. https://doi.org/10.3233/CLO-2009-0501.
36. Bhatt AB, Gupta M, Hoang VT, Chakrabarty S, Wright TD, Elliot S, Chopra IK, Monlish D, Anna K, Burow ME, Cavanaugh JE, Flaherty PT. 2019. Novel diphenylamine analogs induce mesenchymal to epithelial transition in triple negative breast cancer. Front Oncol 9:672. https://doi.org/10.3389/fonc.2019.00672.
37. Peerapen P, Thongboonkerd V. 2020. Protective roles of trigonelline against oxalate-induced epithelial-to-mesenchymal transition in renal tubular epithelial cells: an in vitro study. Food Chem Toxicol 135:110915. https://doi.org/10.1016/j.fct.2019.110915.
38. Nilsson JA, Maclean KH, Keller UB, Pendeville H, Baudino TA, Cleveland JL. 2004. Mnt loss triggers Myc transcription targets, proliferation, apoptosis, and transformation. Mol Cell Biol 24:1560–1569. https://doi.org/10.1128/MCB.24.4.1560-1569.2004.
39. Terragni J, Nayak G, Banerjee S, Medrano J-L, Graham JR, Brennan JF, Sepulveda S, Cooper GM. 2011. The E-box binding factors Max/Mnt, MITF, and USF1 act coordinately with FoxO to regulate expression of proapoptotic and cell cycle control genes by phosphatidylinositol 3-kinase/Akt/glycogen synthase kinase 3 signaling. J Biol Chem 286:36215–36227. https://doi.org/10.1074/jbc.M111.246116.
40. Takayanagi T, Eguchi A, Takaguri A, Hinoki A, Bourne AM, Elliott KJ, Hurlin PJ, Eguchi S. 2013. A repressor protein, Mnt, is a novel negative regulator of vascular smooth muscle cell hypertrophy by angiotensin II and neointimal hyperplasia by arterial injury. Atherosclerosis 228:90–93. https://doi.org/10.1016/j.atherosclerosis.2013.02.033.
41. Yin J, Hu W, Fu W, Dai L, Jiang Z, Zhong S, Deng B, Zhao J. 2019. HGF/MET regulated epithelial-mesenchymal transitions and metastasis by FOSL2 in non-small cell lung cancer. Oncol Targets Ther 12:9227–9237. https://doi.org/10.2147/OTT.S217595.
42. Du X, Pan Z, Li Q, Liu H, Li Q. 2018. SMAD4 feedback regulates the canonical TGF-β signaling pathway to control granulosa cell apoptosis. Cell Death Dis 9:151. https://doi.org/10.1038/s41419-017-0205-2.
43. Zhao J, Geng L, Duan G, Xu W, Cheng Y, Huang Z, Zhou Z, Gong S. 2018. REC8 inhibits EMT by downregulating EGR1 in gastric cancer cells. Oncol Rep 39:1583–1590. https://doi.org/10.3892/or.2018.6244.
44. Hyttinen JMT, Kannan R, Felszeghy S, Niittykoski M, Salminen A, Kaarniranta K. 2019. The regulation of NFE2L2 [NRF2] signaling and epithelial-to-mesenchymal transition in age-related macular degeneration pathology. Int J Mol Sci 20:5800. https://doi.org/10.3390/ijms20225800.
45. Piñero J, Ramírez-Anguita JM, Saüch-Pitarch J, Ronzano F, Centeno E, Sanz F, Furlong LI. 2020. The DisGeNET knowledge platform for disease genomics: 2019 update. Nucleic Acids Res 48:D845–D855. https://doi.org/10.1093/nar/gkz1021.
46. Tyagi S, Gupta P, Saini AS, Kaushal C, Sharma S. 2011. The peroxisome proliferator-activated receptor: a family of nuclear receptors role in various diseases. J Adv Pharm Technol Res 2:236–240. https://doi.org/10.4103/2231-4040.90879.
47. ENCODE Project Consortium. 2012. An integrated encyclopedia of DNA elements in the human genome. Nature 489:57–74. https://doi.org/10.1038/nature11247.
48. Lin X-L, Liu M, Liu Y, Hu H, Pan Y, Zou W, Fan X, Hu X. 2018. Transforming growth factor β1 promotes migration and invasion in HepG2 cells: epithelial-to-mesenchymal transition via JAK/STAT3 signaling. Int J Mol Med 41:129–136. https://doi.org/10.3892/ijmm.2017.3228.

49. Hurlin PJ, Huang J. 2006. The MAX-interacting transcription factor network. Semin Cancer Biol 16:265–274. https://doi.org/10.1016/j.semcancer.2006.07.009.
50. Hurlin PJ, Queva C, Eisenman RN. 1997. Mnt, a novel Max-interacting protein is coexpressed with Myc in proliferating cells and mediates repression at Myc binding sites. Genes Dev 11:44–58. https://doi.org/10.1101/gad.11.1.44.
51. Oughtred R, Rust J, Chang C, Breitkreutz BJ, Stark C, Willems A, Boucher L, Leung G, Kolas N, Zhang F, Dolma S, Coulombe-Huntington J, Chatr-Aryamontri A, Dolinski K, Tyers M. 2021. The BioGRID database: a comprehensive biomedical resource of curated protein, genetic, and chemical interactions. Protein Sci 30:187–200. https://doi.org/10.1002/pro.3978.
52. Wang Z, Zang C, Cui K, Schones DE, Barski A, Peng W, Zhao K. 2009. Genome-wide mapping of HATs and HDACs reveals distinct functions in active and inactive genes. Cell 138:1019–1031. https://doi.org/10.1016/j.cell.2009.06.049.
53. Saha RN, Pahan K. 2006. HATs and HDACs in neurodegeneration: a tale of disconcerted acetylation homeostasis. Cell Death Differ 13:539–550. https://doi.org/10.1038/sj.cdd.4401769.
54. Milazzo G, Mercatelli D, Di Muzio G, Triboli L, De Rosa P, Perini G, Giorgi FM. 2020. Histone deacetylases [HDACs]: evolution, specificity, role in transcriptional complexes, and pharmacological actionability. Genes 11:556. https://doi.org/10.3390/genes11050556.
55. Song C, Pan X, Ge Z, Gowda C, Ding Y, Li H, Li Z, Yochum G, Muschen M, Li Q, Payne KJ, Dovat S. 2016. Epigenetic regulation of gene expression by Ikaros, HDAC1 and Casein Kinase II in leukemia. Leukemia 30:1436–1440. https://doi.org/10.1038/leu.2015.331.
56. Kidder BL, Palmer S. 2012. HDAC1 regulates pluripotency and lineage specific transcriptional networks in embryonic and trophoblast stem cells. Nucleic Acids Res 40:2925–2939. https://doi.org/10.1093/nar/gkr1151.
57. Zeisberg M, Neilson EG. 2009. Biomarkers for epithelial-mesenchymal transitions. J Clin Invest 119:1427–1437.
58. Lavin DP, Tiwari VK. 2020. Unresolved complexity in the gene regulatory network underlying EMT. Front Oncol 10:554. https://doi.org/10.3389/fonc.2020.00554.
59. Ban CR, Twigg SM. 2008. Fibrosis in diabetes complications: pathogenic mechanisms and circulating and urinary markers. Vasc Health Risk Manag 4:575–596. https://doi.org/10.2147/vhrm.s1991.
60. Patel S, Srivastava S, Singh MR, Singh D. 2019. Mechanistic insight into diabetic wounds: pathogenesis, molecular targets and treatment strategies to pace wound healing. Biomed Pharmacother 112:108615. https://doi.org/10.1016/j.biopha.2019.108615.
61. Travers JG, Kamal FA, Robbins J, Yutzey KE, Blaxall BC. 2016. Cardiac fibrosis: the fibroblast awakens. Circ Res 118:1021–1040. https://doi.org/10.1161/CIRCRESAHA.115.306565.
62. Rout-Pitt N, Farrow N, Parsons D, Donnelley M. 2018. Epithelial mesenchymal transition (EMT): a universal process in lung diseases with implications for cystic fibrosis pathophysiology. Respir Res 19:136. https://doi.org/10.1186/s12931-018-0834-8.
63. Li X, Udager AM, Hu C, Qiao XT, Richards N, Gumucio DL. 2009. Dynamic patterning at the pylorus: formation of an epithelial intestine-stomach boundary in late fetal life. Developmental dynamics: an official publication of the. Dev Dyn 238:3205–3217. https://doi.org/10.1002/dvdy.22134.
64. Haber AL, Biton M, Rogel N, Herbst RH, Shekhar K, Smillie C, Burgin G, Delorey TM, Howitt MR, Katz Y, Tirosh I, Beyaz S, Dionne D, Zhang M, Raychowdhury R, Garrett WS, Rozenblatt-Rosen O, Shi HN, Yilmaz O, Xavier RJ, Regev A. 2017. A single-cell survey of the small intestinal epithelium. Nature 551:333–339. https://doi.org/10.1038/nature24489.
65. Nath A, Chan C. 2016. Genetic alterations in fatty acid transport and metabolism genes are associated with metastatic progression and poor prognosis of human cancers. Sci Rep 6:18669. https://doi.org/10.1038/srep18669.
66. Toyo-Oka K, Hirotsune S, Gambello MJ, Zhou ZQ, Olson L, Rosenfeld MG, Eisenman R, Hurlin P, Wynshaw-Boris A. 2004. Loss of the Max-interacting protein Mnt in mice results in decreased viability, defective embryonic growth and craniofacial defects: relevance to Miller-Dieker syndrome. Hum Mol Genet 13:1057–1067. https://doi.org/10.1093/hmg/ddh116.
67. Yingling J, Toyo-Oka K, Wynshaw-Boris A. 2003. Miller-Dieker syndrome: analysis of a human contiguous gene syndrome in the mouse. Am J Hum Genet 73:475–488. https://doi.org/10.1086/378096.
68. Cerami E, Gao J, Dogrusoz U, Gross BE, Sumer SO, Aksoy BA, Jacobsen A, Byrne CJ, Heuer ML, Larsson E, Antipin Y, Reva B, Goldberg AP, Sander C, Schultz N. 2012. The cBio cancer genomics portal: an open platform for exploring multidimensional cancer genomics data. Cancer Discov 2:401–404. https://doi.org/10.1158/2159-8290.CD-12-0095.
69. Gao J, Aksoy BA, Dogrusoz U, Dresdner G, Gross B, Sumer SO, Sun Y, Jacobsen A, Sinha R, Larsson E, Cerami E, Sander C, Schultz N. 2013. Integrative analysis of complex cancer genomics and clinical profiles using the cBioPortal. Sci Signal 6:pl1. https://doi.org/10.1126/scisignal.2004088.
70. Dubois V, Staels B, Lefebvre P, Verzi MP, Eeckhoute J. 2020. Control of cell identity by the nuclear receptor HNF4 in organ pathophysiology. Cells 9:2185. https://doi.org/10.3390/cells9102185.
71. Toyo-Oka K, Bowen TJ, Hirotsune S, Li Z, Jain S, Ota S, Escoubet-Lozach L, Lozach LE, Garcia-Bassets I, Bassett IG, Lozach J, Rosenfeld MG, Glass CK, Eisenman R, Ren B, Hurlin P, Wynshaw-Boris A. 2006. Mnt-deficient mammary glands exhibit impaired involution and tumors with characteristics of myc overexpression. Cancer Res 66:5565–5573. https://doi.org/10.1158/0008-5472.CAN-05-2683.
72. Campbell KJ, Vandenberg CJ, Anstee NS, Hurlin PJ, Cory S. 2017. Mnt modulates Myc-driven lymphomagenesis. Cell Death Differ 24:2117–2126. https://doi.org/10.1038/cdd.2017.131.
73. Panicker V, Cluett C, Shields B, Murray A, Parnell KS, Perry JRB, Weedon MN, Singleton A, Hernandez D, Evans J, Durant C, Ferrucci L, Melzer D, Saravanan P, Visser TJ, Ceresini G, Hattersley AT, Vaidya B, Dayan CM, Frayling TM. 2008. A common variation in deiodinase 1 gene DIO1 is associated with the relative levels of free thyroxine and triiodothyronine. J Clin Endocrinol Metab 93:3075–3081. https://doi.org/10.1210/jc.2008-0397.
74. Brayman M, Thathiah A, Carson DD. 2004. MUC1: a multifunctional cell surface component of reproductive tissue epithelia. Reprod Biol Endocrinol 2:4. https://doi.org/10.1186/1477-7827-2-4.
75. Medina-Gomez G, Gray S, Vidal-Puig A. 2007. Adipogenesis and lipotoxicity: role of peroxisome proliferator-activated receptor gamma [PPARgamma] and PPARgammacoactivator-1 [PGC1]. Public Health Nutr 10:1132–1137. https://doi.org/10.1017/S1368980007000614.
76. Vella V, Nicolosi ML, Giuliano S, Bellomo M, Belfiore A, Malaguarnera R. 2017. PPAR-γ agonists as antineoplastic agents in cancers with dysregulated IGF axis. Front Endocrinol 8:31–31. https://doi.org/10.3389/fendo.2017.00031.
77. Gupta D, Kono T, Evans-Molina C. 2010. The role of peroxisome proliferator-activated receptor γ in pancreatic β cell function and survival: therapeutic implications for the treatment of type 2 diabetes mellitus. Diabetes Obes Metab 12:1036–1047. https://doi.org/10.1111/j.1463-1326.2010.01299.x.
78. Hummler E, Beermann F. 2000. Scnn1 sodium channel gene family in genetically engineered mice. J Am Soc Nephrol 11:S129–S134. https://doi.org/10.1681/ASN.V11suppl_2s129.
79. Pey AL, Megarity CF, Timson DJ. 2019. NAD[P]H quinone oxidoreductase (NQO1): an enzyme which needs just enough mobility, in just the right places. Biosci Rep 39:BSR2018045. https://doi.org/10.1042/BSR20180459.
80. Leth-Larsen R, Garred P, Jensenius H, Meschi J, Hartshorn K, Madsen J, Tornoe I, Madsen HO, Sørensen G, Crouch E, Holmskov U. 2005. A common polymorphism in the SFTPD gene influences assembly, function, and concentration of surfactant protein D. J Immunol 174:1532–1538. https://doi.org/10.4049/jimmunol.174.3.1532.
81. González-Guerrico AM, Cafferata EG, Radrizzani M, Marcucci F, Gruenert D, Pivetta OH, Favaloro RR, Laguens R, Perrone SV, Gallo GC, Santa-Coloma TA. 2002. Tyrosine kinase c-Src constitutes a bridge between cystic fibrosis transmembrane regulator channel failure and MUC1 overexpression in cystic fibrosis. J Biol Chem 277:17239–17247. https://doi.org/10.1074/jbc.M112456200.
82. Kumar R, González-Prieto R, Xiao Z, Verlaan-de Vries M, Vertegaal ACO. 2017. The STUbL RNF4 regulates protein group SUMOylation by targeting the SUMO conjugation machinery. Nat Commun 8:1809–1809. https://doi.org/10.1038/s41467-017-01900-x.
83. Chanda A, Chan A, Deng L, Kornaga EN, Enwere EK, Morris DG, Bonni S. 2017. Identification of the SUMO E3 ligase PIAS1 as a potential survival biomarker in breast cancer. PLoS One 12:e0177639. https://doi.org/10.1371/journal.pone.0177639.
84. Jang SM, Kim CH, Kim JW, Choi KH. 2015. Transcriptional regulatory network of SOX4 during myoblast differentiation. Biochem Biophys Res Commun 462:365–370. https://doi.org/10.1016/j.bbrc.2015.04.142.
85. Cardner M, Meyer-Schaller N, Christofori G, Beerenwinkel N. 2019. Inferring signaling dynamics by integrating interventional with observational data. Bioinformatics 35:i577–i585. https://doi.org/10.1093/bioinformatics/btz325.
86. Trapnell C, Williams BA, Pertea G, Mortazavi A, Kwan G, van Baren MJ, Salzberg SL, Wold BJ, Pachter L. 2010. Transcript assembly and quantification by RNA-Seq reveals unannotated transcripts and isoform switching

during cell differentiation. Nat Biotechnol 28:511–515. https://doi.org/10.1038/nbt.1621.
87. Anders S, Huber W. 2010. Differential expression analysis for sequence count data. Genome Biol 11:R106. https://doi.org/10.1186/gb-2010-11-10-r106.
88. Huang da W, Sherman BT, Lempicki RA. 2009. Systematic and integrative analysis of large gene lists using DAVID bioinformatics resources. Nat Protoc 4:44–57. https://doi.org/10.1038/nprot.2008.211.
89. Huang da W, Sherman BT, Lempicki RA. 2009. Bioinformatics enrichment tools: paths toward the comprehensive functional analysis of large gene lists. Nucleic Acids Res 37:1–13. https://doi.org/10.1093/nar/gkn923.
90. Langmead B, Salzberg SL. 2012. Fast gapped-read alignment with Bowtie 2. Nat Methods 9:357–359. https://doi.org/10.1038/nmeth.1923.
91. Zhang Y, Liu T, Meyer CA, Eeckhoute J, Johnson DS, Bernstein BE, Nusbaum C, Myers RM, Brown M, Li W, Liu XS. 2008. Model-based analysis of ChIP-Seq [MACS]. Genome Biol 9:R137. https://doi.org/10.1186/gb-2008-9-9-r137.
92. Gaidatzis D, Lerch A, Hahne F, Stadler MB. 2015. QuasR: quantification and annotation of short reads in R. Bioinformatics 31:1130–1132. https://doi.org/10.1093/bioinformatics/btu781.
93. Heinz S, Benner C, Spann N, Bertolino E, Lin YC, Laslo P, Cheng JX, Murre C, Singh H, Glass CK. 2010. Simple combinations of lineage-determining transcription factors prime cis-regulatory elements required for macrophage and B cell identities. Mol Cell 38:576–589. https://doi.org/10.1016/j.molcel.2010.05.004.
94. Maeda M, Johnson KR, Wheelock MJ. 2005. Cadherin switching: essential for behavioral but not morphological changes during an epithelium-to-mesenchyme transition. J Cell Sci 118:873–887. https://doi.org/10.1242/jcs.01634.
95. Jacobsen A, Luna A. 2019. Package 'cgdsr': R-based API for accessing the MSKCC Cancer Genomics Data Server (CGDS). https://cran.r-project.org/web/packages/cgdsr/cgdsr.pdf.
96. Wei T, Simko V. 2021. R package 'corrplot': visualization of a correlation matrix, version 0.90. https://github.com/taiyun/corrplot.
97. Lou L, Diao L, Cuentas ERP, Denning WL, Chen L, Fan YH, Byers LA, Wang J, Papadimitrakopoulou VA, Behrens C, Rodriguez JC, Hwu P, Wistuba II, Heymach JV, Gibbons DL. 2016. Epithelial–mesenchymal transition is associated with a distinct tumor microenvironment Including elevation of inflammatory signals and multiple immune checkpoints in lung adenocarcinoma. 22:3630–3642. https://doi.org/10.1158/1078-0432.CCR-15-1434.
98. Kolde R. 2019. Package 'pheatmap': pretty heatmaps. https://cran.r-project.org/web/packages/pheatmap/pheatmap.pdf.